CORONAVIRUS

# Spleen tyrosine kinase inhibition restores myeloid homeostasis in COVID-19

**Gustaf Wigerblad[1], Seth A. Warner[2], Marcos J. Ramos-Benitez[2,3,4], Lela Kardava[5], Xin Tian[6], Rui Miao[6], Robert Reger[7], Mala Chakraborty[7], Susan Wong[7], Yogendra Kanthi[8], Anthony F. Suffredini[2], Stefania Dell'Orso[9], Stephen Brooks[10], Christopher King[11], Oksana Shlobin[11], Steven D. Nathan[11], Jonathan Cohen[12], Susan Moir[5], Richard W. Childs[7,13], Mariana J. Kaplan[1], Daniel S. Chertow[2,5,13], Jeffrey R. Strich[2,13]***



**Spleen tyrosine kinase (SYK) is a previously unidentified therapeutic target that inhibits neutrophil and macrophage activation in coronavirus disease 2019 (COVID-19). Fostamatinib, a SYK inhibitor, was studied in a phase 2 placebo-controlled randomized clinical trial and was associated with improvements in many secondary end points related to efficacy. Here, we used a multiomic approach to evaluate cellular and soluble immune mediator responses of patients enrolled in this trial. We demonstrated that SYK inhibition was associated with reduced neutrophil activation, increased circulation of mature neutrophils ($CD10^+CD33^-$), and decreased circulation of low-density granulocytes and polymorphonuclear myeloid-derived suppressor cells ($HLA\text{-}DR^-CD33^+CD11b^-$). SYK inhibition was also associated with normalization of transcriptional activity in circulating monocytes relative to healthy controls, an increase in frequency of circulating nonclassical and $HLA\text{-}DR^{hi}$ classical monocyte populations, and restoration of interferon responses. Together, these data suggest that SYK inhibition may mitigate proinflammatory myeloid cellular and soluble mediator responses thought to contribute to immunopathogenesis of severe COVID-19.**

## INTRODUCTION

Severe acute respiratory syndrome coronavirus 2 (SARS-CoV-2) has led to a global pandemic resulting in millions of deaths worldwide. A hallmark of coronavirus disease 2019 (COVID-19) pathogenesis is a dysregulated immune response and thromboinflammation contributing to acute respiratory distress syndrome (ARDS) and multisystem organ failure (*1*). Early during the pandemic, elevated neutrophil counts and neutrophil-to-lymphocyte ratios were noted to associate with disease severity (*2*–*6*). There has since been increasing evidence that innate myeloid dysfunction contributes to COVID-19 pathogenesis. High levels of neutrophil biomarkers including S100 calcium binding protein A9 (S100A9), neutrophil gelatinase-associated lipocalin (NGAL)/lipocalin-2 (LCN2), and resistin (RETN) have been associated with disease severity and mortality (*7*, *8*). Furthermore, elevated levels of circulating neutrophil extracellular traps (NETs) have been observed in severe COVID-19 and are thought to promote thromboinflammation and worsen outcomes (*9*, *10*). Single-cell transcriptomics and high-dimensional flow cytometric analyses have revealed more pre-/proimmature neutrophils expressing high levels of genes associated with neutrophil degranulation and NET formation in patients with severe disease along with lower proportions of nonclassical and higher $HLA\text{-}DR^-$ monocytes (*11*, *12*). These findings indicate that severe COVID-19 is associated with the mobilization of immature neutrophils and monocytes from the bone marrow into circulation, indicative of emergency myelopoiesis. Included among these immature populations are low-density granulocytes (LDGs) and myeloid-derived suppressor cells (MDSCs), both of which have been hypothesized to contribute to pathogenesis in COVID-19 and other infections causing critical illness (*13*–*17*).

Spleen tyrosine kinase (SYK), a previously unidentified drug target in critical illness, is a cytoplasmic kinase that binds to immunoreceptor tyrosine-based activation motif (ITAM) of Fc receptors, C-type lectin receptors (CLECs), and B cell receptors (BCRs). Fostamatinib is a SYK inhibitor that is hypothesized to hamper Fc-mediated activation of neutrophils, macrophages, and platelets, ultimately decreasing the risk of thromboinflammation in COVID-19. Preclinical data have demonstrated that fostamatinib is able to inhibit the release of NETs by healthy neutrophils stimulated with COVID-19 plasma, as well as spike antigen/antibody complex–mediated activation of macrophages and platelets (*18*–*21*).

On the basis of its unique mechanisms of action and preclinical data, fostamatinib was evaluated in a phase 2 placebo-controlled randomized clinical trial (*22*). This trial met its primary end point, with serious adverse events occurring in 10.5% of patients who were randomized to fostamatinib and 22% randomized to

[1]Systemic Autoimmunity Branch, National Institute of Arthritis and Musculoskeletal and Skin Disease, Bethesda, MD, USA. [2]Critical Care Medicine Department, National Institutes of Health Clinical Center, Bethesda, MD, USA. [3]Postdoctoral Research Associate Training Program, National Institute of General Medical Sciences, Bethesda, MD, USA. [4]Ponce Health Science University and Ponce Research Institute, Department of Basic Sciences, School of Medicine, Ponce, Puerto Rico, USA. [5]Laboratory of Immunoregulation, National Institute of Allergy and Infectious Diseases, National Institutes of Health (NIH), Bethesda, MD, USA. [6]Office of Biostatistics Research, National Heart, Lung, and Blood Institute, NIH, Bethesda, MD, USA. [7]Laboratory of Transplantation Immunotherapy, National Heart, Lung, and Blood Institute, NIH, Bethesda, MD, USA. [8]Laboratory of Vascular Thrombosis and Inflammation, National Heart, Lung, and Blood Institute, NIH, Bethesda, MD, USA. [9]Genomic Technology Section, National Institute of Arthritis and Musculoskeletal and Skin Diseases, National Institutes of Health, Bethesda, MD, USA. [10]Biodata Mining and Discovery Section, National Institute of Arthritis and Musculoskeletal and Skin Diseases, National Institutes of Health, Bethesda, MD, USA. [11]Advanced Lung Disease and Lung Transplant Program, Inova Fairfax Hospital, Falls Church, VA, USA. [12]Adventist Healthcare Shady Grove Medical Center, Rockville, MD, USA. [13]United States Public Health Service Commissioned Corps, Rockville, MD, USA.
*Corresponding author. Email: jeffrey.strich@nih.gov

placebo. While the small sample size precludes conclusions on efficacy, many secondary end points including mean change in ordinal scale at day 15, days in the intensive care unit, and time on oxygen favored the fostamatinib arm. In addition, numerous biomarkers, including C-reactive protein (CRP) and D-dimer, appeared to have more rapid reductions in the fostamatinib arm, and in an exploratory analysis, there was a trend toward a greater reduction in NETs from day baseline to day 5 in the fostamatinib arm.

In the current study, we sought to understand differences in the myeloid response among those who received fostamatinib versus placebo for the treatment of hospitalized patients on oxygen with COVID-19. First, we used single-cell RNA sequencing (scRNA-seq) to evaluate the myeloid response in COVID-19 compared to healthy controls. We then assessed differences in neutrophil and lymphocyte counts across both arms using clinical data, followed by a multiomic analysis combining transcriptomics (scRNA-seq) and proteomics [cellular indexing of transcriptomes and epitopes by sequencing (CITE-seq)], high-dimensional flow cytometry analysis, and measurement of soluble biomarkers to compare differences in the myeloid compartment in those treated with fostamatinib versus placebo (Fig. 1A).

## RESULTS

### COVID-19 is associated with a dysregulated myeloid compartment

To characterize the putative pathogenic role of myeloid cells in COVID-19, we performed scRNA-seq on baseline samples (before study drug) from seven patients and compared them to six age-matched healthy controls (Fig. 1A). In total, we analyzed 37,300 cells from COVID-19 patients and 40,200 from healthy controls (Fig. 1B and fig. S1, A to C). Uniform manifold approximation and projection (UMAP) analysis demonstrated an increase in the percentage of neutrophils from 50 to 62% of total cells, while lymphocytes decreased from 25 to 10% in COVID-19 patients compared to healthy volunteers (fig. S1, B and D). In addition, the proportion of monocytes among total cells increased from 5 to 23% in COVID-19 patients (fig. S1D). We identified that clusters 12 and 21 in the UMAP were unique to COVID-19 patients and likely represented pre-B cells by increased expression of immunoglobulin genes and *MZB1* (fig. S1, A and C). Population 26 was another distinct population, consisting of precursor neutrophils that highly express granule genes such as lactoferrin (*LTF*), resistin (*RETN*), and lipocalin-2 (*LCN2*), which was elevated in COVID-19 patients versus healthy controls (Fig. 1, C and D). Comparison of gene transcripts that were differentially expressed in COVID-19 revealed that most lineages were affected to some degree; however, those most affected belonged to the innate myeloid compartment (neutrophils and monocytes) (Fig. 1E). Specific pathway analysis demonstrated similar results, as the genes most up-regulated in COVID-19 were associated with innate immune responses, regulation of viral entry, defense responses to bacterium and fungus, cytokine-mediated signaling and responses, and neutrophil functional responses (Fig. 1, F and G). Interferon (IFN)–stimulated gene (ISG) scores (Fig. 1H) and nuclear factor κB (NF-κB) activity (Fig. 1I) were also elevated in COVID-19 samples and localized primarily to the myeloid compartment (fig. S1E). Collectively, these findings support the hypothesis that COVID-19 leads to a hyperactive myeloid response with increased numbers of precursor neutrophils.

### More accelerated resolution of neutrophilia and lymphopenia associated with SYK inhibition

The mean baseline absolute neutrophil count (ANC) and absolute lymphocyte count (ALC) were similar between the fostamatinib and placebo groups; baseline mean ANC (±SE) was 7.66 ± 0.65 K/μl in the fostamatinib arm and 8.81 ± 0.82 K/μl in the placebo arm, while the mean ALC was 0.92 ± 0.07 K/μl versus 0.88 ± 0.09 K/μl, respectively (Fig. 2, A and E). Mean ANC at baseline (before study drug administration) was higher in patients with severe or critical illness compared to mild illness (8.40 K/μl versus 5.54 K/μl, $P = 0.0002$). Neutrophilia normalized earlier in the fostamatinib arm (day 11) compared with the placebo arm (day 15), with a significantly lower mean neutrophil count in the fostamatinib arm on multiple days compared to placebo (8.19 K/μl versus 11.1 K/μl, $P = 0.03$ on day 8; 5.47 K/μl versus 6.65 K/μl, $P = 0.03$ on day 15) (Fig. 2A). Among patients with severe or critical illness, significantly lower mean ANC was observed at days 8, 11, and 15 in the fostamatinib arm (Fig. 2B). SYK inhibition was associated with a lower peak immature granulocyte count compared to placebo, a finding that was more pronounced in patients with severe or critical illness (Fig. 2, C and D). Last, lymphopenia trended toward earlier resolution in the fostamatinib group compared to placebo (Fig. 2E), with a significantly lower ANC-to-ALC ratio observed in the fostamatinib group at day 15 ($P = 0.01$) (Fig. 2F).

### Fostamatinib treatment is associated with a shift in neutrophils to a more mature population and decreased activation

Next, we explored the impact of fostamatinib treatment on neutrophil homeostasis by performing scRNA-seq on fresh whole blood collected on study days 1 and 5 (Fig. 1A). Accordingly, these analyses were performed in real time before knowing the treatment arm associated with each sample. Four of the patients studied were treated with fostamatinib [two had severe disease (ordinal scale 6) at baseline], while three were in the placebo arm (one with severe disease at baseline) (table S1). Analysis of neutrophil populations on day 1, before the first study drug administration, revealed similar proportions of neutrophils (fig. S2A) and minimal transcriptional differences (fig. S2B) between the fostamatinib and placebo groups.

Evaluating day 5 samples, neutrophil populations were divided into nine different clusters with distinct transcriptional profiles (Fig. 3, A and B). Cluster 6 expressed genes associated with precursor neutrophils (*S100A11*, *LTF*, *LCN2*, and *CD24*) (Fig. 3B) and *PADI4*, previously linked to NET formation (fig. S2C). Comparison of these clusters by treatment arm demonstrated significant shifts in neutrophil transcription profiles in fostamatinib- versus placebo-treated patients (Fig. 3C), with a trend toward a reduction in the proportion of cluster 6 precursor cells in the fostamatinib arm (Fig. 3D). In trajectory analysis, to visualize transcriptional state changes along an inferred time, patients treated with fostamatinib transitioned from relatively immature cluster 4 to the more mature cluster 1 (Fig. 3E). Cluster 4 represented immature neutrophils expressing granule genes and *PADI4* (fig. S2C), while cluster 1 was relatively transcriptionally quiescent (fig. S2D), consistent with mature neutrophils that express fewer genes but display high levels of *lncRNA NEAT1* (Fig. 3B) (*23*). Despite being mature neutrophils, cluster 1 nonetheless expressed several genes indicating inflammatory activation, such as *IL1R2* and *PLCG2* (Fig. 3B). In the

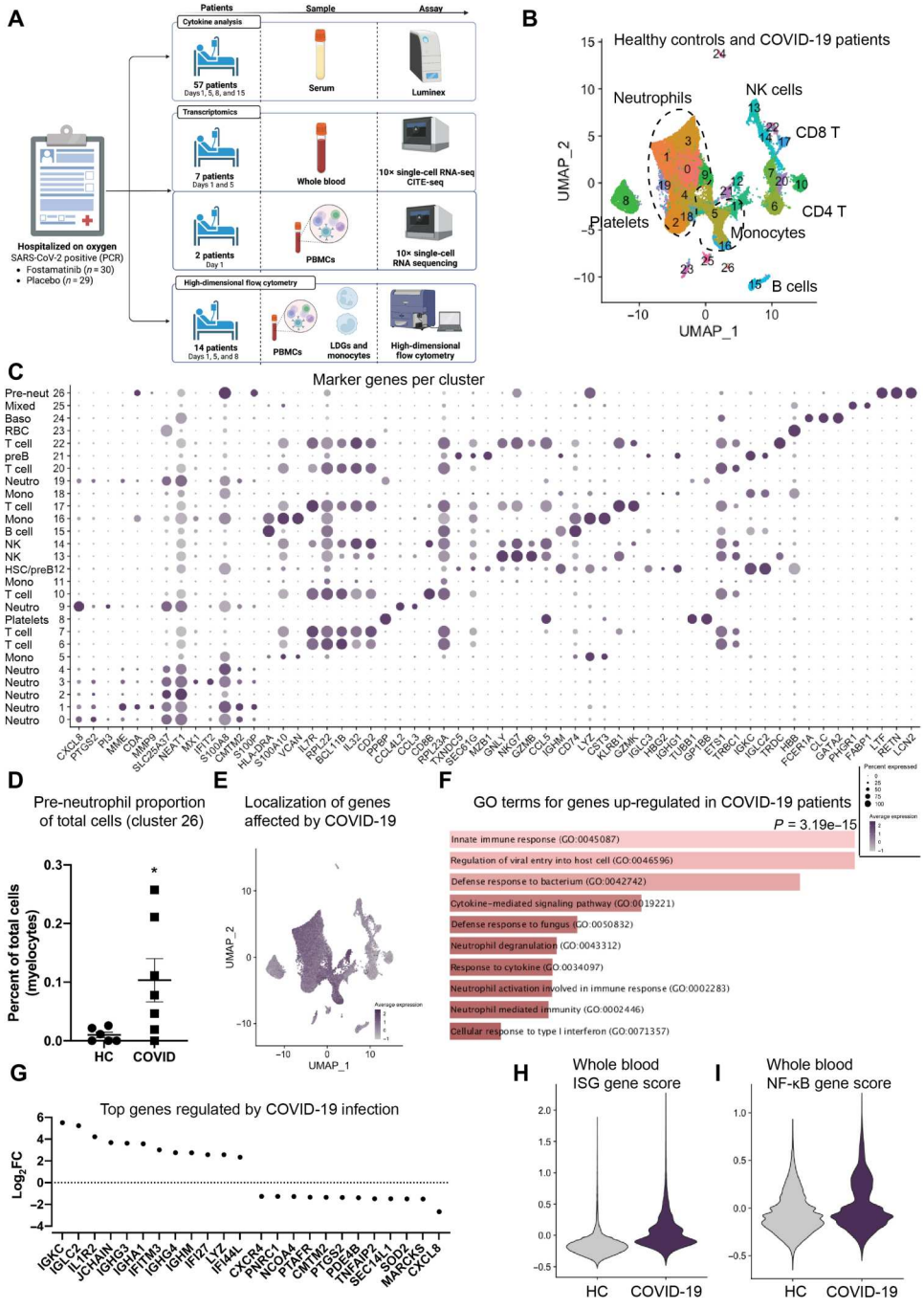


**Fig. 1. Study design and whole blood scRNA-seq at inclusion of the study.** (**A**) Experimental design and setup. Soluble biomarkers were analyzed in 57 patients on days 1, 5, 8, and 15 using the Luminex platform. Whole blood was red blood cell (RBC)–depleted, and cells were captured for scRNA-seq and CITE-seq on days 1 and 5 using the 10x Genomics platform. In two patients, PBMCs were also analyzed using scRNA-seq. PBMCs were additionally analyzed using high-dimensional flow cytometry on days 1, 5, and 8. (**B**) UMAP of RBC-depleted whole blood cells from COVID-19 patients (37,300 cells, seven patients) and healthy controls (40,200 cells, six donors), with major cell types annotated. (**C**) Dot plot showing the top three differentially expressed genes per cluster showing percent expressed and average expression. Population 21 noted to classify as pre-B cells with a mix of hematopoietic stem cells (HSC). (**D**) Percent of precursor neutrophils (myelocytes, cluster 26) of total cells for healthy controls (HC) and COVID-19 patients. (**E**) Localization on the UMAP of the top up-regulated genes between healthy control and COVID-19 patients. (**F**) Gene ontology (GO) terms for the genes used in (E). (**G**) Top regulated genes ($log_2FC$; up or down) between healthy control and COVID-19 patients. (**H**) ISG score for all cells comparing healthy control and COVID-19 patients. (**I**) NF-κB gene score comparing healthy controls to COVID-19.

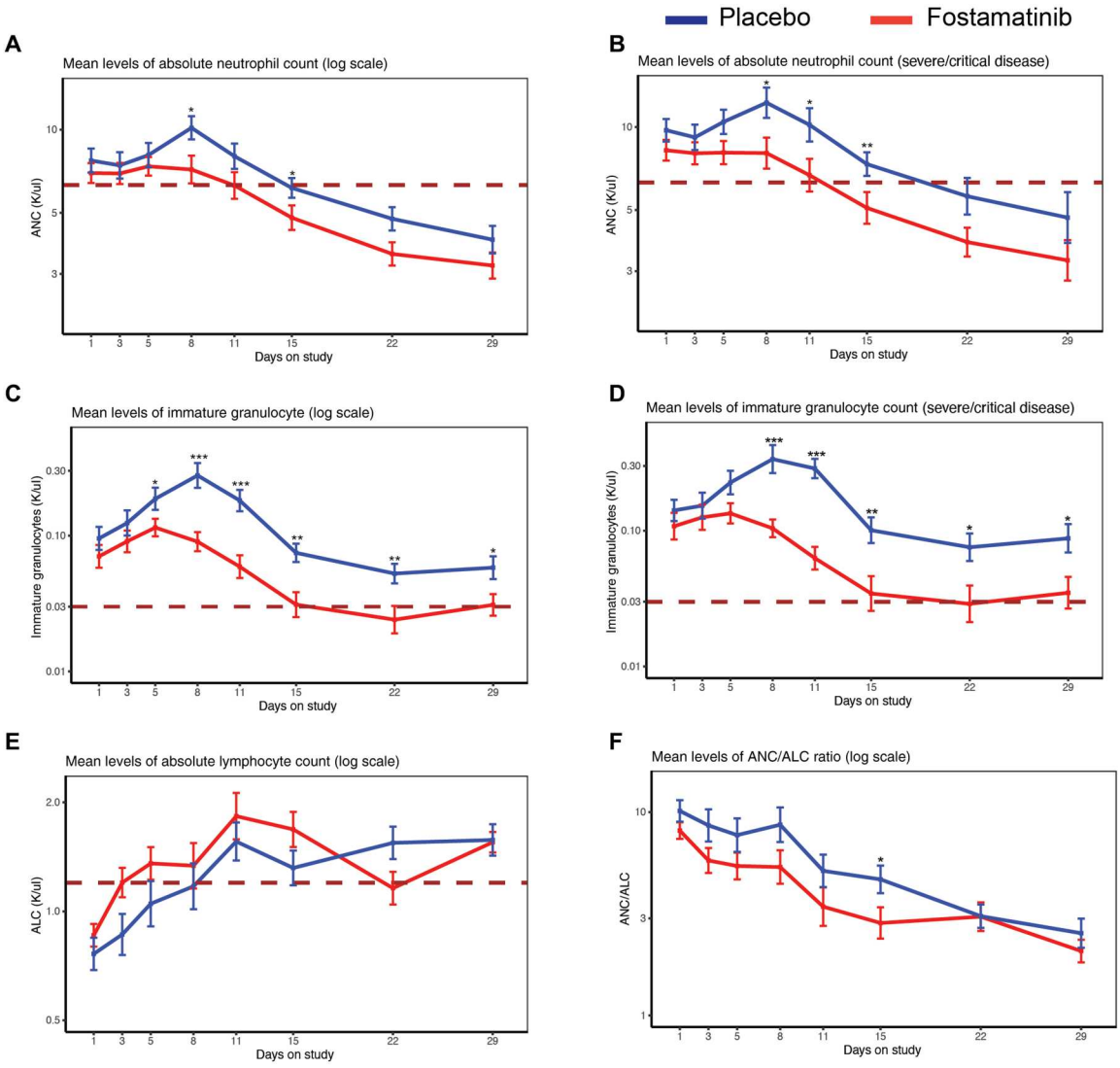


**Fig. 2. Comparisons of neutrophil and lymphocyte counts by complete blood count.** (**A**) ANC (K/μl) per treatment arm for all patients ($n = 59$) or (**B**) for severe disease ($n = 36$). (**C**) Immature granulocyte count (K/μl) per treatment arm for all patients ($n = 59$) or (**D**) for severe disease ($n = 36$). (**E**) ALC (K/μl) per treatment arm for all patients ($n = 59$). (**F**) Ratio of ANC and ALC (ANC/ALC; $n = 59$). Dashed lines on all figures represent normal value [(A and B) ANC (6.3 K/μl), (C and D) immature granulocyte count (0.3 K/μl), and (E) ALC (1.2 K/μl)]. *$P < 0.05$, **$P < 0.01$, and ***$P < 0.001$.

placebo group, this trajectory was shifted (through clusters 0 and 3) but ended in the same cluster 1 (Fig. 3E). This shift was driven in large part by genes associated with neutrophil activation (Fig. 3F) and viral defense like *AIF1* and *IFITM2*, which were accordingly down-regulated in the fostamatinib group (Fig. 3B). Furthermore, the neutrophils in cluster 0 still expressed several granule genes such as *S100A6* and *S100A11*, suggesting that these cells are transcriptionally immature but in an activated state (Fig. 3B).

Fostamatinib treatment was associated with normalized inflammatory gene signatures and resulted in cells that were transcriptionally more analogous to those of healthy controls (Fig. 3G). The four individual genes most down-regulated by fostamatinib were *LTF*, secretory leukocyte protease inhibitor (*SLPI*), *LCN2*, and *RETN*, genes associated with immature neutrophils (Fig. 3H). Furthermore, fostamatinib treatment was associated with slightly higher induction of ISGs (Fig. 3I) but had minimal impact on NF-κB signaling (fig. S2E) in neutrophils, suggesting a continued activated state but a potentially improved antiviral response.

We then evaluated cell surface markers using CITE-seq and found that fostamatinib treatment was associated with more mature neutrophil populations with higher surface expression of CD16, CD10, and CD11b compared to placebo, supporting our prior observation using scRNA-seq that SYK inhibition was associated with a decrease in the number of circulating neutrophil precursor cells (population 6) and fewer immature granulocytes (fig. S2F). In addition to lower surface expression of maturity markers, the placebo group was characterized by increased expression of the precursor marker CD64, adhesion receptor CD31, and complement receptor CD21, indicating that fostamatinib attenuated the immature activated granulocyte phenotype induced by COVID-19.

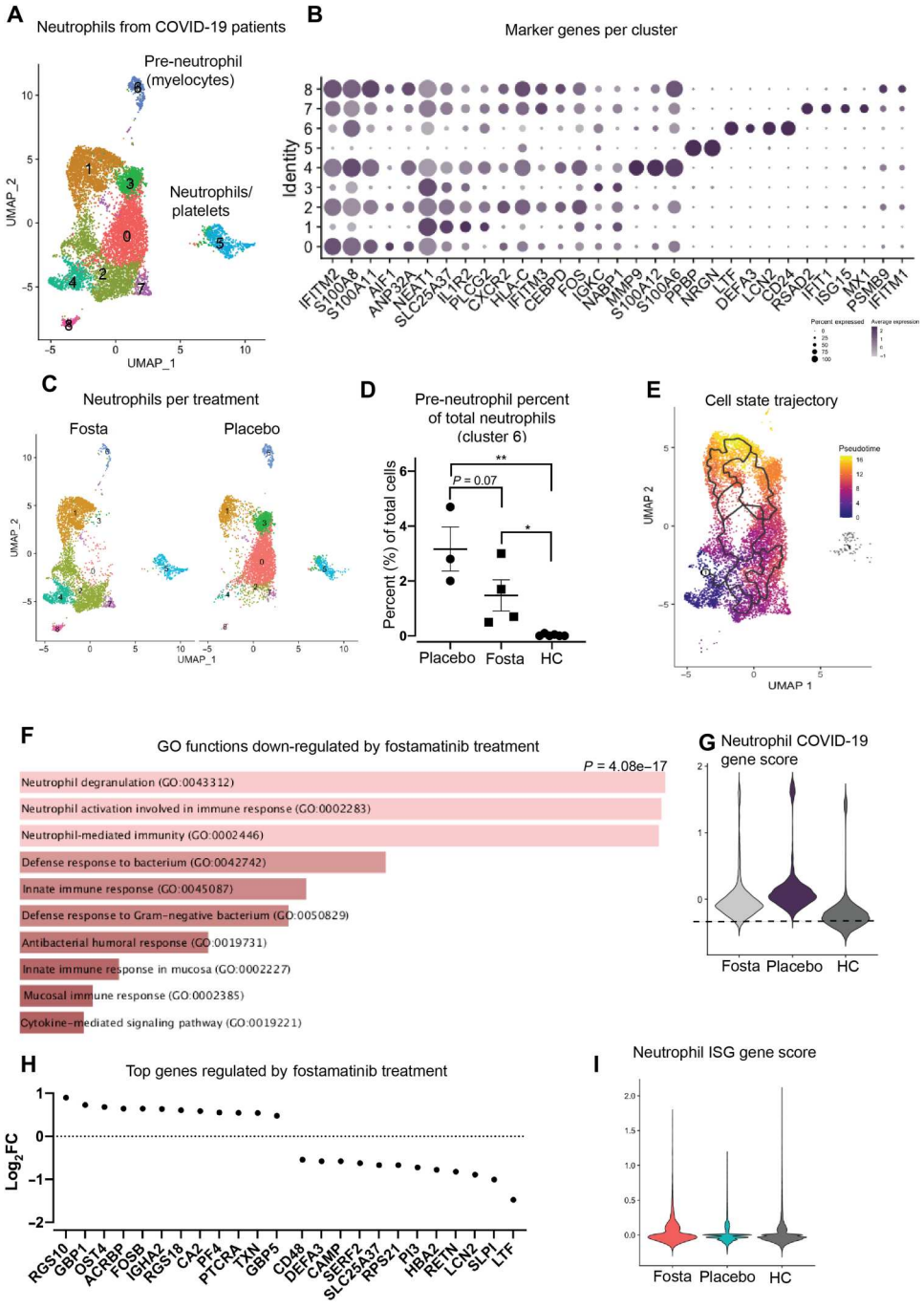


**Fig. 3. Effect of fostamatinib treatment on neutrophils in COVID-19.** (**A**) UMAP of neutrophils on day 5 of treatment with placebo or fostamatinib (corresponds to clusters 0 to 4, 9, 19, and 26 in Fig. 1B). (**B**) Dot plot showing top differentially expressed genes per cluster showing percent expressed and average expression. (**C**) Split UMAP of neutrophils by treatment arm [fostamatinib (Fosta) or placebo]. (**D**) Percent of precursor neutrophils (myelocytes) of total neutrophils comparing treatment arms to healthy controls (HC). (**E**) Trajectory analysis showing cell-state transitions over the neutrophil UMAP, colored with inferred pseudotime. The starting point for the pseudotime is the MMP9$^{high}$ and S100A12$^{high}$ immature neutrophil cluster 4. (**F**) GO terms for the genes that are down-regulated by fostamatinib treatment in the total neutrophils, compared to placebo. (**G**) Neutrophil COVID-19 gene score; gene score based on the top up-regulated genes in neutrophils from COVID-19 neutrophils compared to healthy control neutrophils, applied to each treatment arm and healthy control cells. (**H**) Top regulated genes ($log_2$FC, up or down) among neutrophils by treatment arm. (**I**) ISG score for neutrophils comparing the treatment arm with healthy control cells. *$P$ < 0.05 and **$P$ < 0.01.

### Fostamatinib treatment is associated with lower levels of soluble neutrophil-associated biomarkers

Patients who were randomized to the fostamatinib arm had numerous biomarkers associated with neutrophil activation that normalized more rapidly compared to the placebo arm (fig. S3). At day 8, we found lower levels of LCN2/NGAL (median, 118,071 pg/ml versus 160,192 pg/ml; $P = 0.041$; fig. S3A) across all patients and a trend toward lower interleukin-8 (IL-8) (median, 8.68 pg/ml versus 11.02 pg/ml; $P = 0.055$; fig. S3B) in the fostamatinib arm. We found lower levels of soluble LTF (median, 575,564 pg/ml versus 1,400,600 pg/ml; $P = 0.0004$) and LCN2 (median, 91,712 pg/ml versus 151,550 pg/ml; $P < 0.0001$) at day 15 across all patients; a finding was consistent across the subgroup of patients with moderate disease and severe/critical disease (fig. S3, A and C). For calprotectin (S100A8/S100A9), we found lower levels of S100A9 (median, 2208 pg/ml versus 3235 pg/ml; $P = 0.046$) in those with severe/critical disease at day 15 compared to placebo (fig. S3E).

### Fostamatinib associated with lower proportion of LDGs and PMN-MDSCs

To assess the LDG fraction, we performed high-dimensional flow cytometry on peripheral blood mononuclear cells (PBMCs) from 14 patients (8 on fostamatinib and 6 on placebo) (Fig. 1A). The proportion of LDGs was similar at baseline between both groups (9% versus 13%) (Fig. 4A). However, while the proportion of LDGs trended up between day 1 and day 8 in the placebo group, the LDG fraction remained stable in the fostamatinib group (30% versus 14% at day 8) (Fig. 4A). The LDG populations could be broadly divided into two main clusters based on surface markers (Fig. 4B), representing immature and mature cells. The immature cluster was defined by higher expression of CD33 (Siglec-3) and degranulation marker CD63 (Fig. 4C) and by lack of maturation markers (CD10, CD16, CD32, and CD11b) (Fig. 4D), while the mature cluster showed the opposite expression pattern. At day 8, we found a trend toward lower levels of immature LDGs (42% versus 17%; $P = 0.07$) (Fig. 4C) and higher levels of mature LDG (48% versus 82%; $P = 0.048$) (Fig. 4D) in the fostamatinib arm compared to placebo. In addition, we found higher levels of surface CD62L (L-selectin) in the LDGs of fostamatinib-treated patients ($P = 0.03$) at day 8 (Fig. 4D). It has been suggested that LDGs that are HLA-DR$^-$, CD11b$^+$, CD33$^+$ are immunosuppressive and characteristic of polymorphonuclear MDSC (PMN-MDSC) (*24*). We confirmed the presence of these cells in the LDG fraction and found that the proportion of MDSCs remained relatively stable in the placebo arm; however, fostamatinib treatment was associated with marked reduction in MDSCs by day 8 ($P = 0.03$) (Fig. 4E).

In addition to immunophenotyping, we performed scRNA-seq on the PBMCs of two patients who did not receive fostamatinib and characterized the LDG fraction at the transcriptional level (Fig. 1A). Cluster analysis showed four LDG populations (Fig. 4F). Clusters 0 and 3 likely represent immature neutrophils expressing more granule-associated genes, such as *S100A12* and *MMP9*, while clusters 1 and 2 are transcriptionally similar expressing few genes (Fig. 4, G and H) (*23*). In addition, immature cell clusters 0 and 3 expressed higher levels of Arginase-1 (*Arg-1*) (Fig. 4I) and had a higher gene signature indicative of MDSCs (Fig. 4J) (*25*). To compare the transcriptional profile of the LDGs with normal density neutrophils (NDGs), we performed reclustering of the LDGs with all neutrophils from COVID-19 patients (fig. S4, A and B). We found that these relatively immature MDSC-enriched LDGs expressing *ARG-1* primarily clustered within NDG clusters 0 and 4 (fig. S4, C and D). About half the LDGs clustered separately from NDGs, primarily within cluster 3, driven by up-regulation of adhesion and migration genes like *RACK1*, *VCAN*, and *CD52* (fig. S4, D and E). We found that the proportion of neutrophils that classified as MDSC$^{high}$ demonstrated a trend toward a lower proportion in the fostamatinib arm versus placebo ($P = 0.06$) (fig. S4F).

### Monocyte activation is decreased in the fostamatinib group

High-dimensional flow cytometry analysis was performed on PBMCs from 14 patients (8 on fostamatinib and 6 on placebo) (Fig. 1A) to identify classical (CD14$^{hi}$ CD16$^{lo}$), intermediate (CD14$^{hi}$ CD16$^{int}$), and nonclassical (CD14$^{lo}$ CD16$^{hi}$) monocyte populations (Fig. 5A). We observed similar trends in classical and intermediate monocyte populations in the placebo and fostamatinib groups over time. In contrast, we observed an increase in the percent of nonclassical monocytes at day 8 ($P = 0.02$) in the fostamatinib group, reaching almost 4% of total monocytes (Fig. 5B). Furthermore, the proportion of HLA-DR$^-$ monocytes was stable in the placebo group during the study period, while fostamatinib treatment was associated with an increase in the HLA-DR$^+$ classical monocytes ($P = 0.03$) and a trend toward higher HLA-DR$^+$ nonclassical monocytes ($P = 0.08$) (Fig. 5B).

Single-cell transcriptomic analysis of monocytes on day 1 revealed that both groups displayed an elevated proportion of monocytes compared to healthy controls (fig. S5A) and minimal transcriptional differences in monocyte populations between treatment groups (fig. S5B). Evaluating day 5 samples, we identified five clusters of monocytes (clusters 0 to 4) (Fig. 5C). Treatment with fostamatinib was associated with a large transcriptional shift from clusters 0 and 2 into clusters 1 and 3 (Fig. 5C), driven by genes associated with cytokine production/signaling and proliferation (Fig. 5D and fig. S5C). Fostamatinib treatment was also associated with increased expression of the master inhibitory regulators *DUSP1* and *BTG2* in some monocytes (population 3), suggesting a shift to a less-inflammatory state (Fig. 5E).

The analysis of cell surface protein expression of monocytes on day 5 using CITE-seq revealed changes based on treatment that were consistent with the immunophenotyping of PBMCs. Compared to the fostamatinib group, monocytes from the placebo group displayed lower levels of HLA-DR, CD11c, and CD62L (Fig. 5F). Cluster 2 was CD16$^{hi}$ (Fig. 5F) and expressed genes associated with activation like *NAMPT* and *LITAF* (Fig. 5E), which was largely absent after fostamatinib treatment (Fig. 5C). Fostamatinib treatment was associated with a normalization in the COVID-19 monocyte gene score (Fig. 5G), along with a restoration of antiviral ISG responses (Fig. 5, H and I), largely attributable to CD11c$^{lo}$ CD62L$^{lo}$ HLA-DR$^{med}$ cluster 1 monocytes (Fig. 5J). In addition, we found that fostamatinib was associated with a slight decrease in NF-κB signaling compared to placebo (fig. S5D).

### Fostamatinib is associated with lower levels of soluble biomarkers of monocyte function and NF-κB activation

Patients who were randomized to the fostamatinib arm had numerous biomarkers associated with monocyte function that normalized more rapidly compared to the placebo arm (fig. S6). CXCL1 was lower at day 8 in the fostamatinib arm when evaluating all patients (median, 1757 pg/ml versus 2273 pg/ml; $P = 0.045$) (fig. S6A), while

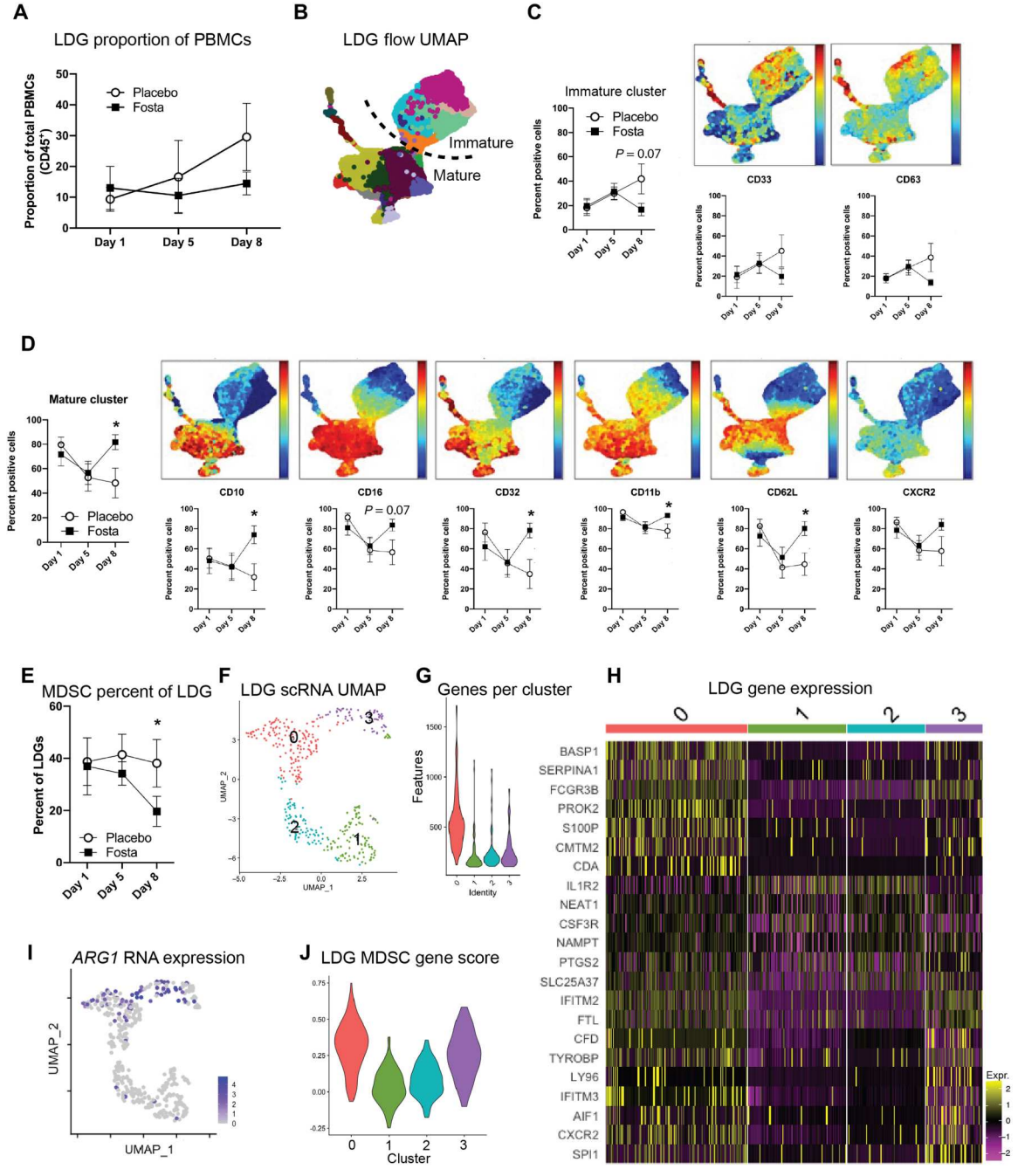


**Fig. 4. High-dimensional flow and scRNA analysis of COVID-19 LDGs.** (**A**) Proportion of LDGs among total CD45$^+$ PBMCs by treatment arm (fostamatinib or placebo) from baseline to day 8. (**B**) UMAP and FlowSOM clustering based on a 24-marker panel (dashed line represents separation of mature and immature populations). (**C**) Markers defining the immature population with percent positive cell per immature cluster and each individual surface marker. (**D**) Markers defining the mature population with percent positive cell per mature cluster and each individual surface marker. (**E**) PMN-MDSC (HLA-DR$^-$CD11b$^+$CD33$^+$) percent of total LDG, per treatment arm. (**F**) UMAP of LDGs from COVID-19 patients at baseline ($n = 2$). (**G**) Genes expressed per cluster in four LDG clusters. (**H**) Heatmap showing gene expression of top differentially expressed genes in each LDG cluster. (**I**) Arginase-1 gene expression across the LDG UMAP. (**J**) MDSC gene score per cluster. MDSC$^{hi}$ indicates cells that express high levels of genes characteristic of MDSCs. *$P < 0.05$.

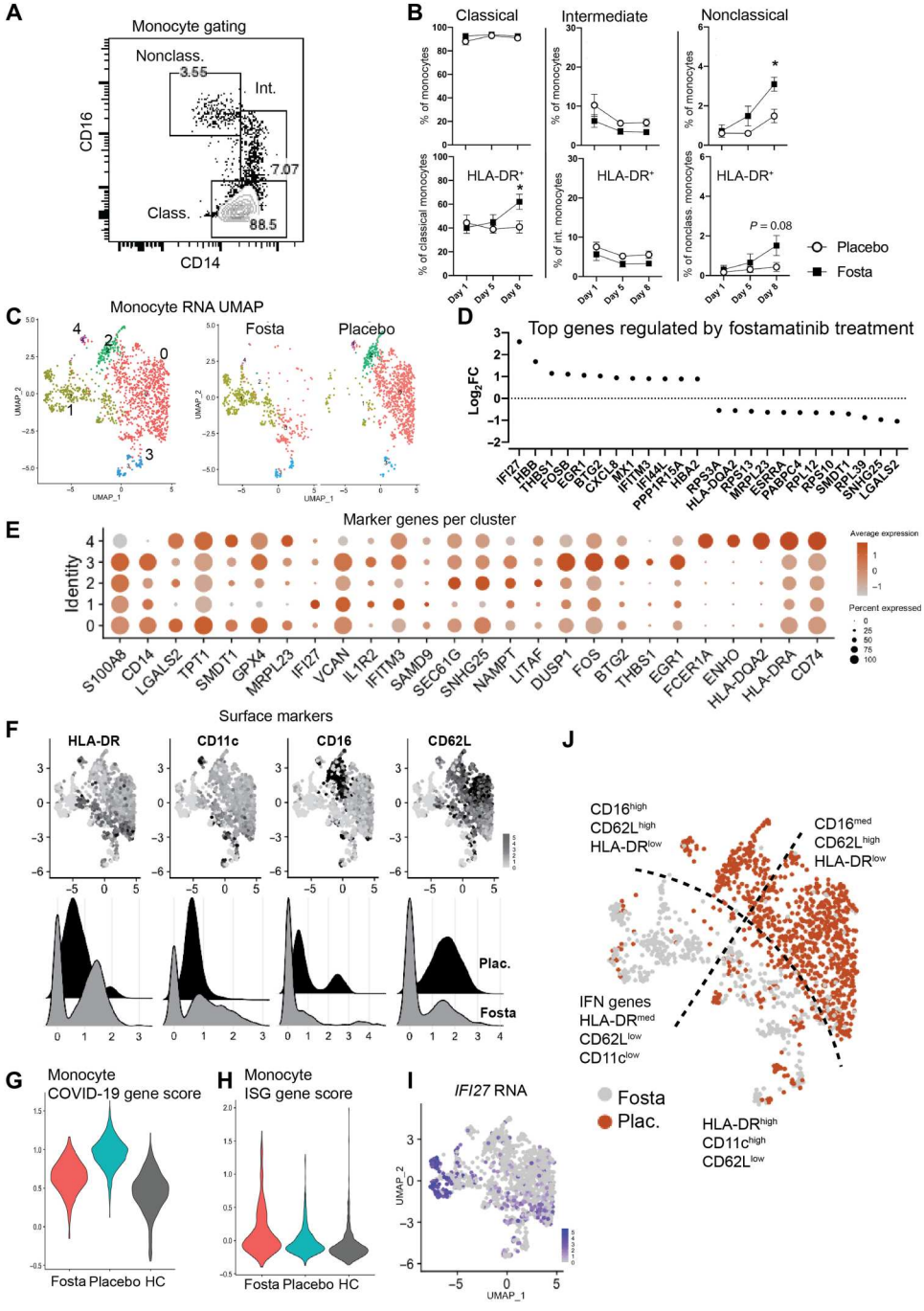


**Fig. 5. Effect of fostamatinib treatment on COVID-19 monocytes.** (**A**) Gating strategy to define classical monocytes ($CD14^{hi}$ $CD16^{lo}$), intermediate monocytes ($CD14^{hi}$ $CD16^{int}$), and nonclassical monocytes ($CD14^{int}$ $CD16^{hi}$). (**B**) Proportion of each monocyte subset of total monocytes (top) by arm (fostamatinib or placebo). Proportion of $HLA\text{-}DR^{+}$ cells in each monocyte subset (bottom). (**C**) UMAP of all monocytes (corresponds to clusters 5, 11, 16, and 18 in Fig. 1B) by treatment arm showing transcriptional clusters (left) and per treatment arm (right). (**D**) Top regulated genes ($log_2FC$; up or down) between the monocytes per treatment arm. (**E**) Dot plot showing top differentially expressed genes per cluster showing percent expressed and average expression. (**F**) CITE-seq of defining surface markers shown on the transcriptional UMAP (top) and comparing per treatment arm (bottom). (**G**) COVID-19 monocyte gene score based on the top up-regulated genes in monocytes from COVID-19 patients compared to healthy controls, applied to each treatment arm and healthy control (HC) cells. (**H**) Gene scores for ISG in the monocytes, comparing the treatment arms with healthy control cells. (**I**) Expression of an ISG gene (*IFI27*) across the UMAP. (**J**) Highlighting surface markers and gene expression that defines the monocytes across the UMAP, including separation by treatment arm. $^{*}P < 0.05$.

IL-6 levels were lower at day 15 in the fostamatinib arm (median, 0.96 pg/ml versus 2.67 pg/ml; $P = 0.031$) when comparing all patients, a difference that was more pronounced in patients with severe/critical disease (median, 0.99 pg/ml versus 3.41 pg/ml; $P = 0.0076$) (fig. S6B). We also found an association between tumor necrosis factor (TNF) signaling and fostamatinib treatment. Specifically, compared to placebo, we noted lower levels of soluble TNF receptor II (TNF-RII) at day 15 in all patients on fostamatinib (median, 2957 pg/ml versus 3800 pg/ml; $P = 0.025$; fig. S6C) and lower levels of TNF-RI in those with severe/critical disease at day 8 (median, 2066 pg/ml versus 2939 pg/ml; $P = 0.033$) and day 15 (median, 1432 pg/ml versus 2317 pg/ml; $P = 0.011$; fig. S6D). Furthermore, fostamatinib treatment was associated with decreases in soluble markers associated with inflammasome activation. IL-1ra was lower in all patients at day 15 (median, 1193 pg/ml versus 2184 pg/ml; $P = 0.0011$) and at day 8 (median, 1495 pg/ml versus 2879 pg/ml; $P = 0.026$) and day 15 (median, 1107 pg/ml versus 2806 pg/ml; $P = 0.0003$) in patients with severe/critical disease (fig. S6E).

### Neutrophil activation predicts response to fostamatinib

Last, we sought to identify biomarkers that could predict which COVID-19 patients may be more likely to respond to SYK inhibition. Among circulating biomarkers associated with neutrophil activation, we found that the fostamatinib arm had a significant interaction with LCN2/NGAL and LTF, while among biomarkers associated with monocyte activation, fostamatinib treatment had a significant interaction with TNF-RII (Fig. 6). For each of these biomarkers, we selected an optimal cutoff level to display their interaction. Among patients with higher baseline levels of LCN2 (>135 pg/μl), the fostamatinib arm had more rapid time to improvement (decrease) by >1 ordinal scale ($P = 0.012$) and a trend toward shorter duration of oxygen use ($P = 0.09$) compared to the placebo arm (Fig. 6, A and B). Similarly, among patients with higher baseline levels of LTF (>1300 pg/μl), the fostamatinib arm was associated with a more rapid improvement in ordinal scale ($P = 0.03$) and a trend toward oxygen requirement ($P = 0.064$) compared to placebo (Fig. 6, C and D). Last, the fostamatinib arm was associated with faster improvement in ordinal scale ($P = 0.017$) and shorter time to wean off oxygen ($P = 0.012$) than placebo among the subgroup of patients with higher baseline levels of TNF-RII (>3.5 pg/μl) (Fig. 6, E and F).

## DISCUSSION

SARS-CoV-2 infection is characterized by a profoundly dysregulated immune response (*3*, *26*–*28*). Despite improved therapeutics, SARS-CoV-2 infection requiring hospitalization is still associated with high mortality (*29*–*31*). Therefore, innovative host-directed therapeutics are urgently needed. Furthermore, translational studies embedded in clinical trials can provide information to better understand mechanisms by which promising therapeutics improve outcomes. Here, we report the results of a multiomic approach investigating the impact of SYK inhibition in COVID-19 and hypothesize how this therapy may alter myeloid responses that contribute to improved outcomes in hospitalized patients requiring supplemental oxygen. Our multiomic approach revealed that patients treated with fostamatinib experienced a decrease in neutrophil activation and a shift from an immature ($CD10^{-}CD33^{+}$) to a more mature neutrophil phenotype ($CD10^{+}CD33^{-}$). Furthermore, SYK inhibition was associated with increased levels of nonclassical monocytes and a classical monocyte population that shifted from primarily $HLA\text{-}DR^{lo}$ to a mixed population of $HLA\text{-}DR^{hi}$, a phenotype associated with mild COVID-19 (*11*).

Severe COVID-19 has been associated with higher levels of immature pre- and pro-neutrophils that are $CD33^{+}CD10^{-}$ (*11*, *12*). In contrast, mild COVID-19 is associated with more mature neutrophil populations that are $CD33^{-}CD10^{+}$. These findings suggest that severe COVID-19 is associated with emergency granulopoiesis (*11*). During emergency granulopoiesis, which has been described in conditions such as infection, sepsis, and trauma, various cytokines [IL-6, granulocyte colony-stimulating factor (G-CSF), and granulocyte-macrophage colony-stimulating factor (GM-CSF)] stimulate bone marrow to release immature neutrophils into circulation (*32*–*34*). These pro- and pre-neutrophils express high levels of genes associated with synthesis of proteins contained in neutrophil granules such as *MPO*, *LCN2*, *LTF*, *RETN*, and *MMP8* and are also characterized by the expression of the surface marker CD33 and absence of CD10 (*8*).

We found that fostamatinib treatment was associated with lower proportions of pre-neutrophils expressing *S100A11*, *LTF*, *LCN2*, *CD24*, and *PADI4*, which encodes for a protein associated with the release of NETs, supporting our prior ex vivo finding that fostamatinib can inhibit NET formation when healthy neutrophils are stimulated with plasma from patients with COVID-19 and our phase 2 clinical trial finding of a trend toward a greater decline in NETs at day 5 in those who received fostamatinib (*2*, *18*, *20*, *21*). This finding was consistent across the different analyses performed, namely, of whole blood neutrophils using scRNA-seq, as well as protein expression by CITE-seq and phenotyping of the LDG fraction among PBMCs. The shift in neutrophil maturation status was also evident when evaluating the immature granulocyte fraction on complete blood counts.

Furthermore, severe COVID-19 has been associated with elevated levels of many soluble biomarkers, including those associated with neutrophil activation such as RETN, NGAL, LTF, and S100A9 (*8*). Here, we demonstrated that fostamatinib treatment was associated with decreased soluble NGAL/LCN2, LTF, and S100A9, supporting the hypothesis that fostamatinib promotes normalization of neutrophil phenotype in COVID-19, resulting in a population of neutrophils that are less activated. Collectively, these findings suggest that fostamatinib modulates emergency granulopoiesis and improves neutrophil homeostasis.

Another feature of emergency granulopoiesis is the release of MDSCs, which are defined by their ability to inhibit the proliferation and activation of lymphocytes (*35*). MDSCs have been described in various infections and are classified into two categories: PMN-MDSC and monocytic MDSC (M-MDSC) (*36*–*38*). Both PMN-MDSC and M-MDSC have been phenotypically identified in COVID-19 and functionally shown to suppress lymphocyte activation and proliferation (*17*, *24*, *39*, *40*). Furthermore, levels of MDSC have been associated with disease severity (*41*). Another cell type not found during normal myeloid homeostasis is LDGs, which are neutrophils found in PBMC fraction of cell isolation and express many genes associated with neutrophil activation, degranulation, and NET formation. They have been described in various infectious and inflammatory diseases and have been associated with disease severity and coagulation in COVID-19 (*42*, *43*).

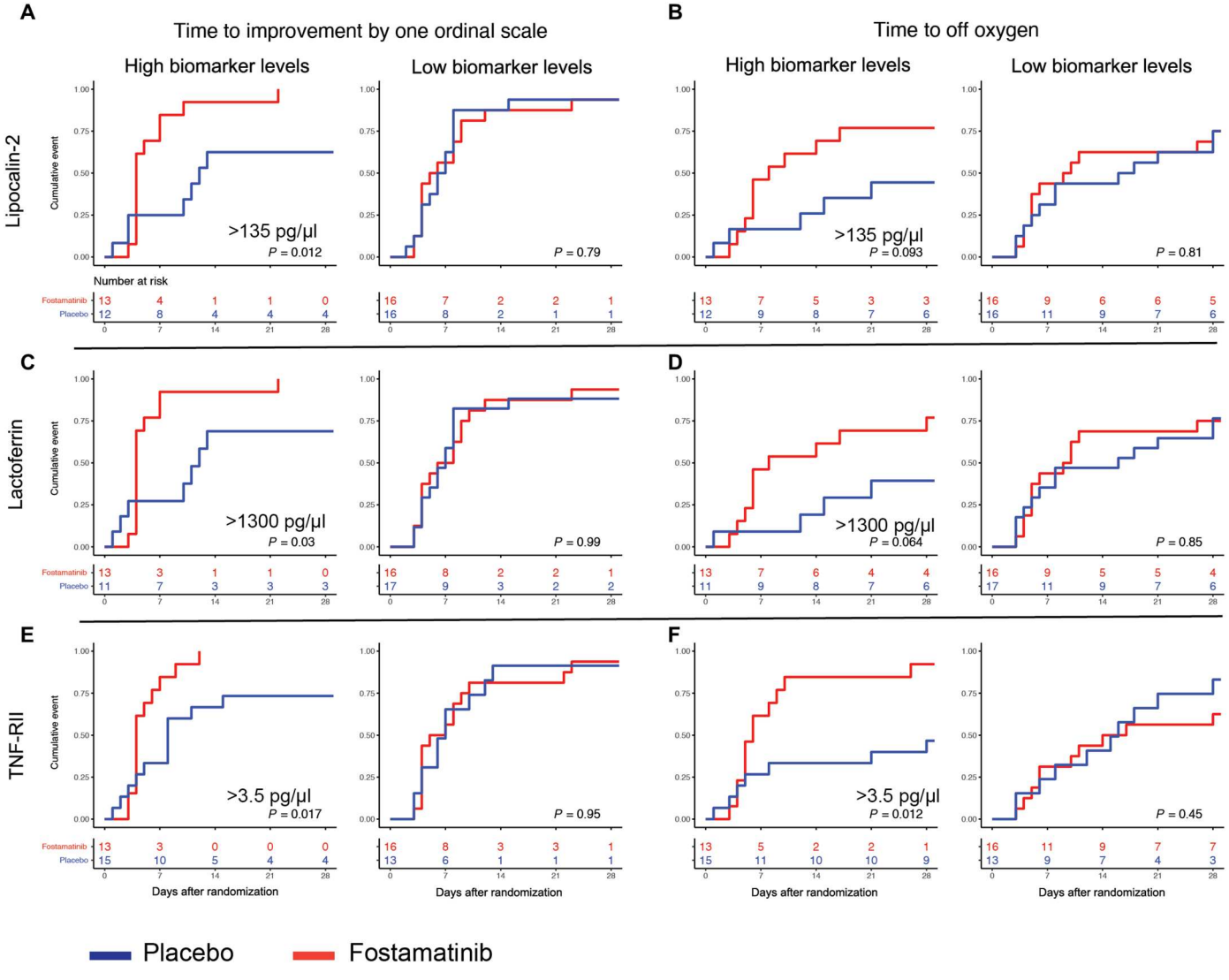


**Fig. 6. Predictive model for fostamatinib indication.** Kaplan-Meier curves demonstrating biomarker cutoffs where higher levels associate with more rapid improvements and lower levels demonstrate no difference in time to improvement by one ordinal scale and time to off oxygen. (**A**) Higher levels of LCN2 (>135 pg/μl) associated with more rapid time to improvement by one ordinal scale. (**B**) Higher level of LCN2 (>135 pg/μl) associated with more rapid time to being off supplemental oxygen. (**C**) Higher levels of LTF (>1300 pg/μl) associated with more rapid time to improvement by one ordinal scale. (**D**) Higher level of LTF (>1300 pg/μl) associated with more rapid time to being off supplemental oxygen. (**E**) Higher levels of TNF-RII (>3.5 pg/μl) associated with more rapid time to improvement by one ordinal scale. (**F**) Higher level of TNF-RII associated (>3.5 pg/μl) with more rapid time to being off supplemental oxygen.

We found that fostamatinib treatment was associated with a decrease in the number of LDGs on day 8 of treatment. Furthermore, within the LDG fraction, we were able to identify a population of cells consistent with PMN-MDSC ($CD11b^+CD33^+$) that decreased from day 1 to day 8 in the fostamatinib arm. Given that these PMN-MDSC have been shown to be immunosuppressive, the decrease in frequency of PMN-MDSC in the fostamatinib arm may explain the concomitant recovery in lymphocyte counts. Moreover, using scRNA-seq from two patients not treated with fostamatinib, we were able to demonstrate two populations (populations 0 and 3) that are transcriptionally immature neutrophils in the LDG fraction that expressed high levels of genes associated with MDSC, including *ARG-1* (*35*). Arginase-1 can sequester arginine and is one mechanism used by PMN-MDSC to inhibit proliferation of lymphocyte. On further analysis, these populations cluster within the normal density granulocyte fraction and we found that fostamatinib treatment was associated with a lower proportion of $MDSC^{high}$ neutrophils. Note that dexamethasone is hypothesized to expand an $ARG1^+$ neutrophil population in COVID-19, raising the potential of fostamatinib as added benefit to steroids (*44*).

In addition to neutrophil dysregulation, severe COVID-19 is associated with abnormalities in the monocyte compartment, including the emergence of HLA-$DR^{lo}$ immunosuppressive monocytes (*40*, *45*, *46*). In contrast, mild COVID-19 is associated with HLA-$DR^{hi}$ monocytes and a robust IFN response. Moreover, severe COVID-19 is associated with a decrease in the number of $CD14^{lo}CD16^{hi}$ nonclassical monocytes (less than 4% of monocytes), which are thought to have anti-inflammatory and antiviral

properties (*47*–*49*). We found that fostamatinib treatment resulted in a shift in the classical monocyte population from HLA-DR$^{lo}$ to HLA-DR$^{hi}$, a finding that may be associated with improved outcomes (*50*–*52*). HLA-DR is a major histocompatibility complex (MHC) class II glycoprotein expressed on antigen-presenting cells and presents peptides from antigens to T cell receptors (*53*). As a result of decreased HLA-DR expression in severe COVID-19, monocytes may be less effective at presenting viral antigens, resulting in decreased T cell activation (*54*). Furthermore, M-MDSCs isolated from patients with COVID-19 have been characterized as CD14$^{+}$HLA-DR$^{-}$ and functionally demonstrated to inhibit T cell proliferation and IFN-γ production (*40*). Hence, the increase in the HLA-DR$^{hi}$ monocytes following fostamatinib treatment may attenuate the immunosuppression that has been associated with COVID-19 (*40*). By analyzing the kinetics of the monocyte populations, we found that at day 8 of fostamatinib treatment, there was an increase in nonclassical monocytes nearing 4% of all monocytes, a finding consistent with mild COVID-19 (*11*). Notably, we also found a subpopulation of monocytes in patients treated with fostamatinib that displayed higher levels of ISGs, indicative of functional antiviral responses. In addition, consistent with the scRNA-seq and CITE-seq data, fostamatinib resulted in a decrease in many soluble biomarkers associated with monocyte activation such as TNF-RI, TNF-RII, and IL-6. IL-6 has been shown to be an important driver of emergency granulopoiesis in sepsis and COVID-19 (*55*). These data across monocyte populations are supported by prior findings that fostamatinib can inhibit the release of cytokines from macrophages stimulated by SARS-CoV-2–specific spike antigen/antibody complexes (*2*, *18*, *20*, *21*). Together, our data suggest that fostamatinib treatment is associated with a decrease in monocyte activation.

Our study has some limitations. First, we had a small sample size for our transcriptional analysis, but our findings were robust and reproducible across all assays applied in this study. Second, we were unable to confirm that the populations we defined as MDSC functionally have this role; however, the functional ability of these populations has been described by others (*24*, *40*). Third, although our findings were robust and consistent, the sequencing data did not include patients on mechanical ventilation; thus, we were unable to test whether changes in the myeloid cells are associated with critical disease. Fourth, we do not have any direct evidence that SYK phosphorylation and downstream signaling were inhibited in this study, and therefore, our findings are inferred from the transcriptional and phenotypic changes found between arms. Last, this phase 2 clinical trial was not intended to provide definitive evidence of efficacy. Note that two phase 3 randomized clinical trials (NCT04629703 and NCT04924660) are ongoing to assess the efficacy of fostamatinib in hospitalized patients with COVID-19, and our observations may help support the use of specific biomarkers in defining likelihood of response to treatment.

Overall, our findings suggest that SYK inhibition is a potential therapeutic target that might improve clinical outcomes in severe COVID-19 by mitigating immunopathogenesis mediated by neutrophils and monocytes. We hypothesize that SYK inhibition decreases emergency granulopoiesis and restores myeloid homeostasis in severe COVID-19 by inhibiting neutrophil and monocyte activation in peripheral blood, inhibiting signals that promote the release of immature immunosuppressive myeloid cells from the bone marrow.

## MATERIALS AND METHODS

### Study cohort

Patients in the current study were part of a larger cohort described in detail in a previous publication (*22*). They were enrolled in a phase 2 randomized, double-blinded, placebo-controlled study evaluating the safety and efficacy of fostamatinib in hospitalized patients with COVID-19 who required oxygen [NCT04579393, National Institutes of Health (NIH) IRB# 000110]. Patients who were ordinal scale 5, 6, or 7 were randomized 1:1 to receive 14 days of fostamatinib (150 mg twice a day) or placebo in addition to standard of care (remdesivir and steroids) (*22*). Patients with moderate disease [ordinal scale 5 (oxygen via nasal canula)] accounted for 39% of the subjects enrolled in the study, while those with severe/critical disease [ordinal scale 6 (oxygen via high-flow oxygen or noninvasive ventilation) or 7 (mechanical ventilation)] accounted for the remaining 61% of the subjects enrolled in the study. Patients on study had research blood drawn on days 1, 5, 8, and 15, in either serum separator tubes (red top) or EDTA (lavender top). ANC and ALC were measured as part of routine clinical tests. One patient who had scRNA-seq performed on LDG fraction of PBMC was enrolled in a COVID-19 natural history study (NCT04401449).

### Luminex biomarker

We measured soluble biomarkers from days 1 (before study drug initiation), 5, 8, and 15 in 57 patients (29 randomized to fostamatinib and 28 to placebo). Plasma samples were analyzed for IL-16, IL-8, lactoferrin, LCN2/NGAL, S100A9, S100A8, IL-18, L-selectin (CD62L), CCL-2 (MCP-1), IL-12, IL-15, CCL-4 (MIP-1β), u-plasminogen activator (uPA), CCL-3 (MIP-1α), CD163, CX3CL-1 (fractalkine), CCL-7 (MCP-3), CCL-8 (MCP-2), GM-CSF, IL-6, TNF-RI, TNF-RII, TNF-α, IL-18, IL-1α, IL-1β, and IL-1ra (R&D Systems, Minneapolis, MN). All assays were performed according to the instructions provided by the manufacturer. Briefly, median fluorescence intensities were collected on a Luminex-200 instrument (Bio-Rad) using Bio-Plex Manager software version 6.2 (Bio-Rad). Standard curves for each cytokine were generated using the premixed lyophilized standards provided in the kits, and cytokine concentrations were determined from the standard curve using a five-point regression to transform the median fluorescence intensity values into concentrations. Each sample was run in duplicate, and the average of the duplicates was used as the measured concentration. Any value that was below detection level was replaced by the limit of detection (LOD) as reported using the Luminex kit. Analyses were performed using Data Pro Manager 1.02 (Bio-Rad). In this study, we report the findings of markers associated with neutrophil activation and monocyte activation, which appeared to have the strongest association with fostamatinib treatment.

### Phenotyping of LDGs and monocytes by flow cytometry

PBMCs were isolated by Ficoll density gradient centrifugation from whole blood collected in EDTA tubes. A 24-color panel was developed to phenotype LDGs by spectral flow cytometry (see table S2 for the list and source of antibodies). A total of $10^6$ freshly isolated PBMCs were incubated in sequence with an Fc receptor blocker (TrueStain FcX, BioLegend) for 15 min at 4°C, the Zombie NIR Fixable Viability Dye (BioLegend) for 10 min at room temperature, and a cocktail containing the panel of antibodies in staining buffer

[2% fetal bovine serum/phosphate-buffered saline (PBS)] supplemented with Brilliant Stain Buffer Plus (BD Biosciences) at 4°C for 15 min. The stained cells were acquired on an Aurora spectral cytometer using SpectroFlo Software v2.2.0 (Cytek Biosciences) and analyzed using FlowJo v10.7.1 (BD Biosciences). Gating strategy to determine LDGs and monocytes is shown in fig. S7.

### UMAP embedding and FlowSOM clustering of spectral flow cytometry data

UMAP embedding and FlowSOM clustering were performed on FCS files generated from spectral flow cytometry using the OMIQ platform (omiq.ai). Live, CD66B$^+$ single cells were selected for downstream analysis. Markers CD66B, CD14, CD15, CD11b, CD10, CD11c, CD16, CD32, CD33, CD62L, CD63, CD107a, CD73, PDL1, PDL2, Lox-1, HLA-DR, CXCR2, CXCR4, CD35, and CD54 were used to perform UMAP embedding and FlowSOM clustering with the number of metaclusters set to 20.

### Single-cell RNA sequencing

The following procedures were previously described. For single-cell sequencing, white blood cells were isolated with the Erythroclear Red Blood Cell Depletion Reagent Kit (STEMCELL Technologies, catalog no. 01738), according to the manufacturer′s protocol. Cells were washed with PBS with 0.02% bovine serum albumin. To obtain single-cell gel beads in emulsion (GEMs), we resuspended cells at a concentration of 1000 cells/μl and loaded the mix on the Chromium Comptroller Instrument (10x Genomics). Single-cell cDNAs and libraries were prepared with Chromium Single-Cell 3′ Library and Gel Bead Kit v3.1 (10x Genomics, catalog no. 1000121). Briefly, GEM-RT incubation was performed in a C1000 Touch thermal cycler with 96-deep well reaction module (Bio-Rad, catalog no. 1851197). Single-strand cDNAs were purified with DynaBeads MyOne Silane Beads (Thermo Fisher Scientific, catalog no. 37002D) and amplified with the C1000 cycler. Amplified cDNA products were cleaned with 0.6X DynaBeads MyOne Silane Beads (Thermo Fisher Scientific, catalog no. 37002D). Quality and quantity of the cDNAs were assessed on 4200 TapeStation (Agilent Technologies) with High Sensitivity D5000 DNA ScreenTape (Agilent, catalog no. 5067-5592). Libraries were diluted to the same molarity and pooled for sequencing on NovaSeq6000 (Illumina) sequencers (*23*).

### Cellular indexing of transcriptomes and epitopes by sequencing

TotalSeq-B oligonucleotide-conjugated antibodies (BioLegend), compatible with the 10x Genomics 3′ scRNA-seq chemistry, were used according to the manufacturer′s protocol. The panel for common markers of circulating neutrophils included antibodies targeting CD45, CD14, CD33, CD11c, CD10, CD16, CD107a, HLA-DR, CD11b, CD66b, CD35, CD24, CD184, and CD15 (*23*).

### Processing and analysis of scRNA-seq data and CITE-seq

Illumina run folders were demultiplexed and converted to FASTQ format with Cell Ranger mkfastq version 4.0.0 and Illumina bcl2fastq version 2.20. Reads were further counted and analyzed with Cell Ranger count version 4.0.0 and the refdata-gex-GRCh38-2020-A reference to generate raw and filtered matrix files.

Matrix files were imported into R package Seurat version 4.0.1 for downstream processing. From the raw matrices, cells with a gene number between 100 and 2500 and a mitochondrial gene proportion of <0.1 were selected for downstream analysis. The matrices were then normalized by the LogNormalize method. The FindVariableFeatures() function was used to select the top 2000 variable genes, with the vst selection method. Scaling was performed by the function ScaleData() regressing out the mitochondrial gene content. Principal components analysis and clustering were then performed on the scaled data. UMAP (version 0.2.7.0) was used for visualization. After cell types were identified using marker genes in the dataset corresponding to each sample, they were integrated. Genes that were shared among all datasets were identified for downstream integration. Anchors were identified with the FindIntegrationAnchors() function, and these anchors were used to integrate the cells together with the function IntegrateData(). To study neutrophil cell–state trajectories, we used the analysis toolkit Monocle3, which is implemented as an R package (version 0.2.3.0). A principal graph was learned on the UMAP projection of the cells with the learn_graph() function. To generate a pseudotime axis, the cells were then ordered with the order_cells() function. To generate gene scores, the function AddModuleScore was used with the indicated gene list and five random control genes per feature used (*23*).

### Statistical analysis

Biomarker data were summarized by means ± SEM or median and compared by the Wilcoxon rank sum test and analysis of variance (ANOVA) between the two treatment groups at each time point. The rate of change for the biomarker over time was compared between treatment groups using the linear mixed model. Cox proportional hazards regression models were used to assess the interaction effect between the treatment arm and the baseline level of biomarkers on the clinical outcomes (improvement by 1 or more points on ordinal scale and requirement for supplemental oxygen), adjusted for the baseline diseases severity. The event rates for clinical outcomes were estimated by the Kaplan-Meier method and compared by the log-rank test. Because of the exploratory nature of the data, no adjustment was made for multiple comparisons. All tests were two sided, and a $P$ value of <0.05 was considered statistically significant. Analysis was performed using the R statistical software, version 4.1.0 (R Foundation for Statistical Computing, Vienna, Austria).

## Supplementary Materials

**This PDF file includes:**

Figs. S1 to S7
Table S1 and S2

## REFERENCES AND NOTES

1. A. Bonaventura, A. Vecchié, L. Dagna, K. Martinod, D. L. Dixon, B. W. van Tassell, F. Dentali, F. Montecucco, S. Massberg, M. Levi, A. Abbate, Endothelial dysfunction and immunothrombosis as key pathogenic mechanisms in COVID-19. *Nat. Rev. Immunol.* **21**, 319–329 (2021).
2. C. Huang, Y. Wang, X. Li, L. Ren, J. Zhao, Y. Hu, L. Zhang, G. Fan, J. Xu, X. Gu, Z. Cheng, T. Yu, J. Xia, Y. Wei, W. Wu, X. Xie, W. Yin, H. Li, M. Liu, Y. Xiao, H. Gao, L. Guo, J. Xie, G. Wang, R. Jiang, Z. Gao, Q. Jin, J. Wang, B. Cao, Clinical features of patients infected with 2019 novel coronavirus in Wuhan, China. *Lancet* **395**, 497–506 (2020).
3. C. Qin, L. Zhou, Z. Hu, S. Zhang, S. Yang, Y. Tao, C. Xie, K. Ma, K. Shang, W. Wang, D.-S. Tian, Dysregulation of immune response in patients with coronavirus 2019 (COVID-19) in Wuhan, China. *Clin. Infect. Dis.* **71**, 762–768 (2020).
4. N. Reusch, E. de Domenico, L. Bonaguro, J. Schulte-Schrepping, K. Baßler, J. L. Schultze, A. C. Aschenbrenner, Neutrophils in COVID-19. *Front. Immunol.* **12**, 652470 (2021).

5. L. Prozan, E. Shusterman, J. Ablin, A. Mitelpunkt, A. Weiss-Meilik, A. Adler, G. Choshen, O. Kehat, Prognostic value of neutrophil-to-lymphocyte ratio in COVID-19 compared with influenza and respiratory syncytial virus infection. *Sci. Rep.* **11**, 21519 (2021).
6. Y. Liu, X. Du, J. Chen, Y. Jin, L. Peng, H. H. X. Wang, M. Luo, L. Chen, Y. Zhao, Neutrophil-to-lymphocyte ratio as an independent risk factor for mortality in hospitalized patients with COVID-19. *J. Infect.* **81**, e6–e12 (2020).
7. M. S. Abers, O. M. Delmonte, E. E. Ricotta, J. Fintzi, D. L. Fink, A. A. A. de Jesus, K. A. Zarember, S. Alehashemi, V. Oikonomou, J. V. Desai, S. W. Canna, B. Shakoory, K. Dobbs, L. Imberti, A. Sottini, E. Quiros-Roldan, F. Castelli, C. Rossi, D. Brugnoni, A. Biondi, L. R. Bettini, M. D'Angio, P. Bonfanti, R. Castagnoli, D. Montagna, A. Licari, G. L. Marseglia, E. F. Gliniewicz, E. Shaw, D. E. Kahle, A. T. Rastegar, M. Stack, K. Myint-Hpu, S. L. Levinson, M. DiNubile, D. W. Chertow, P. D. Burbelo, J. I. Cohen, K. R. Calvo, J. S. Tsang; NIAID COVID-19 Consortium, H. C. Su, J. I. Gallin, D. B. Kuhns, R. Goldbach-Mansky, M. S. Lionakis, L. D. Notarangelo, An immune-based biomarker signature is associated with mortality in COVID-19 patients. *JCI Insight* **6**, e144455 (2021).
8. M. L. Meizlish, A. B. Pine, J. D. Bishai, G. Goshua, E. R. Nadelmann, M. Simonov, C.-H. Chang, H. Zhang, M. Shallow, P. Bahel, K. Owusu, Y. Yamamoto, T. Arora, D. S. Atri, A. Patel, R. Gbyli, J. Kwan, C. H. Won, C. dela Cruz, C. Price, J. Koff, B. A. King, H. M. Rinder, F. P. Wilson, J. Hwa, S. Halene, W. Damsky, D. van Dijk, A. I. Lee, H. J. Chun, A neutrophil activation signature predicts critical illness and mortality in COVID-19. *Blood Adv.* **5**, 1164–1177 (2021).
9. Y. Zuo, S. Yalavarthi, H. Shi, K. Gockman, M. Zuo, J. A. Madison, C. Blair, A. Weber, B. J. Barnes, M. Egeblad, R. J. Woods, Y. Kanthi, J. S. Knight, Neutrophil extracellular traps in COVID-19. *JCI Insight* **5**, e138999 (2020).
10. E. A. Middleton, X.-Y. He, F. Denorme, R. A. Campbell, D. Ng, S. P. Salvatore, M. Mostyka, A. Baxter-Stoltzfus, A. C. Borczuk, M. Loda, M. J. Cody, B. K. Manne, I. Portier, E. S. Harris, A. C. Petrey, E. J. Beswick, A. F. Caulin, A. Iovino, L. M. Abegglen, A. S. Weyrich, M. T. Rondina, M. Egeblad, J. D. Schiffman, C. C. Yost, Neutrophil extracellular traps contribute to immunothrombosis in COVID-19 acute respiratory distress syndrome. *Blood* **136**, 1169–1179 (2020).
11. A. Silvin, N. Chapuis, G. Dunsmore, A.-G. Goubet, A. Dubuisson, L. Derosa, C. Almire, C. Hénon, O. Kosmider, N. Droin, P. Rameau, C. Catelain, A. Alfaro, C. Dussiau, C. Friedrich, E. Sourdeau, N. Marin, T.-A. Szwebel, D. Cantin, L. Mouthon, D. Borderie, M. Deloger, D. Bredel, S. Mouraud, D. Drubay, M. Andrieu, A.-S. Lhonneur, V. Saada, A. Stoclin, C. Willekens, F. Pommeret, F. Griscelli, L. G. Ng, Z. Zhang, P. Bost, I. Amit, F. Barlesi, A. Marabelle, F. Pène, B. Gachot, F. André, L. Zitvogel, F. Ginhoux, M. Fontenay, E. Solary, Elevated calprotectin and abnormal myeloid cell subsets discriminate severe from mild COVID-19. *Cell* **182**, 1401–1418.e18 (2020).
12. J. Schulte-Schrepping, N. Reusch, D. Paclik, K. Baßler, S. Schlickeiser, B. Zhang, B. Krämer, T. Krammer, S. Brumhard, L. Bonaguro, E. de Domenico, D. Wendisch, M. Grasshoff, T. S. Kapellos, M. Beckstette, T. Pecht, A. Saglam, O. Dietrich, H. E. Mei, A. R. Schulz, C. Conrad, D. Kunkel, E. Vafadarnejad, C.-J. Xu, A. Horne, M. Herbert, A. Drews, C. Thibeault, M. Pfeiffer, S. Hippenstiel, A. Hocke, H. Müller-Redetzky, K.-M. Heim, F. Machleidt, A. Uhrig, L. B. de Jarcy, L. Jürgens, M. Stegemann, C. R. Glösenkamp, H.-D. Volk, C. Goffinet, M. Landthaler, E. Wyler, P. Georg, M. Schneider, C. Dang-Heine, N. Neuwinger, K. Kappert, R. Tauber, V. Corman, J. Raabe, K. M. Kaiser, M. T. Vinh, G. Rieke, C. Meisel, T. Ulas, M. Becker, R. Geffers, M. Witzenrath, C. Drosten, N. Suttorp, C. von Kalle, F. Kurth, K. Händler, J. L. Schultze, A. C. Aschenbrenner, Y. Li, J. Nattermann, B. Sawitzki, A.-E. Saliba, L. E. Sander, A. Angelov, R. Bals, A. Bartholomäus, A. Becker, D. Bezdan, E. Bonifacio, P. Bork, T. Clavel, M. Colome-Tatche, A. Diefenbach, A. Dilthey, N. Fischer, K. Förstner, J. S. Frick, J. Gagneur, A. Goesmann, T. Hain, M. Hummel, S. Janssen, J. Kalinowski, R. Kallies, B. Kehr, A. Keller, S. Kim-Hellmuth, C. Klein, O. Kohlbacher, J. O. Korbel, I. Kurth, M. Landthaler, Y. Li, K. Ludwig, O. Makarewicz, M. Marz, A. McHardy, C. Mertes, M. Nöthen, P. Nürnberg, U. Ohler, S. Ossowski, J. Overmann, S. Peter, K. Pfeffer, A. R. Poetsch, A. Pühler, N. Rajewsky, M. Ralser, O. Rieß, S. Ripke, U. N. da Rocha, P. Rosenstiel, A. E. Saliba, L. E. Sander, B. Sawitzki, P. Schiffer, E. C. Schulte, J. L. Schultze, A. Sczyrba, O. Stegle, J. Stoye, F. Theis, J. Vehreschild, J. Vogel, M. von Kleist, A. Walker, J. Walter, D. Wieczorek, J. Ziebuhr, Severe COVID-19 is marked by a dysregulated myeloid cell compartment. *Cell* **182**, 1419–1440.e23 (2020).
13. N. L. Denning, M. Aziz, S. D. Gurien, P. Wang, DAMPs and NETs in sepsis. *Front. Immunol.* **10**, 2536 (2019).
14. R. Kanamaru, H. Ohzawa, H. Miyato, S. Matsumoto, H. Haruta, K. Kurashina, S. Saito, Y. Hosoya, H. Yamaguchi, H. Yamashita, Y. Seto, A. K. Lefor, N. Sata, J. Kitayama, Low density neutrophils (LDN) in postoperative abdominal cavity assist the peritoneal recurrence through the production of neutrophil extracellular traps (NETs). *Sci. Rep.* **8**, 632 (2018).
15. M. F. Denny, S. Yalavarthi, W. Zhao, S. G. Thacker, M. Anderson, A. R. Sandy, W. J. McCune, M. J. Kaplan, A distinct subset of proinflammatory neutrophils isolated from patients with systemic lupus erythematosus induces vascular damage and synthesizes type I IFNs. *J. Immunol.* **184**, 3284–3297 (2010).
16. I. T. Schrijver, E. Karakike, C. Théroude, P. Baumgartner, A. Harari, E. J. Giamarellos-Bourboulis, T. Calandra, T. Roger, High levels of monocytic myeloid-derived suppressor cells are associated with favorable outcome in patients with pneumonia and sepsis with multi-organ failure. *Intensive Care Med. Exp.* **10**, 5 (2022).
17. M. Rowlands, F. Segal, D. Hartl, Myeloid-derived suppressor cells as a potential biomarker and therapeutic target in COVID-19. *Front. Immunol.* **12**, 697405 (2021).
18. J. R. Strich, M. J. Ramos-Benitez, D. Randazzo, S. R. Stein, A. Babyak, R. T. Davey, A. F. Suffredini, R. W. Childs, D. S. Chertow, Fostamatinib inhibits neutrophils extracellular traps induced by COVID-19 patient plasma: A potential therapeutic. *J. Infect. Dis.* **223**, 981–984 (2021).
19. W. Hoepel, H.-J. Chen, C. E. Geyer, S. Allahverdiyeva, X. D. Manz, S. W. de Taeye, J. Aman, L. Mes, M. Steenhuis, G. R. Griffith, P. I. Bonta, P. J. M. Brouwer, T. G. Caniels, K. van der Straten, K. Golebski, R. E. Jonkers, M. D. Larsen, F. Linty, J. Nouta, C. P. A. A. van Roomen, F. E. H. P. van Baarle, C. M. van Drunen, G. Wolbink, A. P. J. Vlaar, G. J. de Bree, R. W. Sanders, L. Willemsen, A. E. Neele, D. van de Beek, T. Rispens, M. Wuhrer, H. J. Bogaard, M. J. van Gils, G. Vidarsson, M. de Winther, J. den Dunnen, High titers and low fucosylation of early human anti-SARS-CoV-2 IgG promote inflammation by alveolar macrophages. *Sci. Transl. Med.* **13**, eabf8654 (2021).
20. S. A. Apostolidis, A. Sarkar, H. M. Giannini, R. R. Goel, D. Mathew, A. Suzuki, A. E. Baxter, A. R. Greenplate, C. Alanio, M. Abdel-Hakeem, D. A. Oldridge, J. R. Giles, J. E. Wu, Z. Chen, Y. J. Huang, J. Belman, A. Pattekar, S. Manne, O. Kuthuru, J. Dougherty, B. Weiderhold, A. R. Weisman, C. A. G. Ittner, S. Gouma, D. Dunbar, I. Frank, A. C. Huang, L. A. Vella; UPenn COVID Processing Unit, J. P. Reilly, S. E. Hensley, L. Rauova, L. Zhao, N. J. Meyer, M. Poncz, C. S. Abrams, E. J. Wherry, Signaling through FcγRIIA and the C5a-C5aR pathway mediate platelet hyperactivation in COVID-19. *Front. Immunol.* **13**, 834988 (2022).
21. A. P. Bye, W. Hoepel, J. L. Mitchell, S. Jégouic, S. Loureiro, T. Sage, G. Vidarsson, J. Nouta, M. Wuhrer, S. de Taeye, M. van Gils, N. Kriek, N. Cooper, I. Jones, J. den Dunnen, J. M. Gibbins, Aberrant glycosylation of anti-SARS-CoV-2 spike IgG is a prothrombotic stimulus for platelets. *Blood* **138**, 1481–1489 (2021).
22. J. R. Strich, X. Tian, M. Samour, C. S. King, O. Shlobin, R. Reger, J. Cohen, K. Ahmad, A. W. Brown, V. Khangoora, S. Aryal, Y. Migdady, J. J. Kyte, J. Joo, R. Hays, A. C. Collins, E. Battle, J. Valdez, J. Rivero, I.-k. Kim, J. Erb-Alvarez, R. Shalhoub, M. Chakraborty, S. Wong, B. Colton, M. J. Ramos-Benitez, S. Warner, D. S. Chertow, K. N. Olivier, G. Aue, R. T. Davey, A. F. Suffredini, R. W. Childs, S. D. Nathan, Fostamatinib for the treatment of hospitalized adults with COVD-19 A randomized trial. *Clin. Infect. Dis.* **75**, e491–e498 (2021).
23. G. Wigerblad, Q. Cao, S. Brooks, F. Naz, M. Gadkari, K. Jiang, S. Gupta, L. O'Neil, S. Dell'Orso, M. J. Kaplan, L. M. Franco, Single-cell analysis reveals the range of transcriptional states of circulating human neutrophils. *J. Immunol.* **209**, 772–782 (2022).
24. C. Agrati, A. Sacchi, V. Bordoni, E. Cimini, S. Notari, G. Grassi, R. Casetti, E. Tartaglia, E. Lalle, A. D'Abramo, C. Castilletti, L. Marchioni, Y. Shi, A. Mariano, J.-W. Song, J.-Y. Zhang, F.-S. Wang, C. Zhang, G. M. Fimia, M. R. Capobianchi, M. Piacentini, A. Antinori, E. Nicastri, M. Maeurer, A. Zumla, G. Ippolito, Expansion of myeloid-derived suppressor cells in patients with severe coronavirus disease (COVID-19). *Cell Death Differ.* **27**, 3196–3207 (2020).
25. H. Alshetaiwi, N. Pervolarakis, L. L. McIntyre, D. Ma, Q. Nguyen, J. A. Rath, K. Nee, G. Hernandez, K. Evans, L. Torosian, A. Silva, C. Walsh, K. Kessenbrock, Defining the emergence of myeloid-derived suppressor cells in breast cancer using single-cell transcriptomics. *Sci. Immunol.* **5**, eaay6017 (2020).
26. P. García-González, F. Tempio, C. Fuentes, C. Merino, L. Vargas, V. Simon, M. Ramirez-Pereira, V. Rojas, E. Tobar, G. Landskron, J. P. Araya, M. Navarrete, C. Bastias, R. Tordecilla, M. A. Varas, P. Maturana, A. E. Marcoleta, M. L. Allende, R. Naves, M. A. Hermoso, F. Salazar-Onfray, M. Lopez, M. R. Bono, F. Osorio, Dysregulated immune responses in COVID-19 patients correlating with disease severity and invasive oxygen requirements. *Front. Immunol.* **12**, 769059 (2021).
27. A. J. Wilk, M. J. Lee, B. Wei, B. Parks, R. Pi, G. J. Martínez-Colón, T. Ranganath, N. Q. Zhao, S. Taylor, W. Becker; Stanford COVID- Biobank, D. Jimenez-Morales, A. L. Blomkalns, R. O'Hara, E. A. Ashley, K. C. Nadeau, S. Yang, S. Holmes, M. Rabinovitch, A. J. Rogers, W. J. Greenleaf, C. A. Blish, Multi-omic profiling reveals widespread dysregulation of innate immunity and hematopoiesis in COVID-19. *J. Exp. Med.* **218**, e20210582 (2021).
28. M. Lourda, M. Dzidic, L. Hertwig, H. Bergsten, L. M. P. Medina, I. Sinha, E. Kvedaraite, P. Chen, J. R. Muvva, J.-B. Gorin, M. Cornillet, J. Emgård, K. Moll, M. García, K. T. Maleki, J. Klingström, J. Michaëlsson, M. Flodström-Tullberg, S. Brighenti, M. Buggert, J. Mjösberg, K.-J. Malmberg, J. K. Sandberg, J.-I. Henter, E. Folkesson, S. Gredmark-Russ, A. Sönnerborg, L. I. Eriksson, O. Rooyackers, S. Aleman, K. Strålin, H.-G. Ljunggren, N. K. Björkström, M. Svensson, A. Ponzetta, A. Norrby-Teglund, B. J. Chambers; Karolinska KI/K COVID-19 Study Group, High-dimensional profiling reveals phenotypic heterogeneity and disease-specific alterations of granulocytes in COVID-19. *Proc. Natl. Acad. Sci. U.S.A.* **118**, e2109123118 (2021).
29. J. H. Beigel, K. M. Tomashek, L. E. Dodd, A. K. Mehta, B. S. Zingman, A. C. Kalil, E. Hohmann, H. Y. Chu, A. Luetkemeyer, S. Kline, D. L. de Castilla, R. W. Finberg, K. Dierberg, V. Tapson, L. Hsieh, T. F. Patterson, R. Paredes, D. A. Sweeney, W. R. Short, G. Touloumi, D. C. Lye, N. Ohmagari, M.-D. Oh, G. M. Ruiz-Palacios, T. Benfield, G. Fätkenheuer, M. G. Kortepeter, R. L. Atmar, C. B. Creech, J. Lundgren, A. G. Babiker, S. Pett, J. D. Neaton, T. H. Burgess,

T. Bonnett, M. Green, M. Makowski, A. Osinusi, S. Nayak, H. C. Lane; ACTT-1 Study Group Members, Remdesivir for the treatment of Covid-19—Final report. *N. Engl. J. Med.* **383**, 1813–1826 (2020).

30. A. C. Kalil, T. F. Patterson, A. K. Mehta, K. M. Tomashek, C. R. Wolfe, V. Ghazaryan, V. C. Marconi, G. M. Ruiz-Palacios, L. Hsieh, S. Kline, V. Tapson, N. M. Iovine, M. K. Jain, D. A. Sweeney, H. M. El Sahly, A. R. Branche, J. R. Pineda, D. C. Lye, U. Sandkovsky, A. F. Luetkemeyer, S. H. Cohen, R. W. Finberg, P. E. H. Jackson, B. Taiwo, C. I. Paules, H. Arguinchona, N. Erdmann, N. Ahuja, M. Frank, M.-D. Oh, E.-S. Kim, S. Y. Tan, R. A. Mularski, H. Nielsen, P. O. Ponce, B. S. Taylor, L. A. Larson, N. G. Rouphael, Y. Saklawi, V. D. Cantos, E. R. Ko, J. J. Engemann, A. N. Amin, M. Watanabe, J. Billings, M.-C. Elie, R. T. Davey, T. H. Burgess, J. Ferreira, M. Green, M. Makowski, A. Cardoso, S. de Bono, T. Bonnett, M. Proschan, G. A. Deye, W. Dempsey, S. U. Nayak, L. E. Dodd, J. H. Beigel; ACTT-2 Study Group Members, Baricitinib plus remdesivir for hospitalized adults with Covid-19. *N. Engl. J. Med.* **384**, 795–807 (2021).
31. The REMAP-CAP Investigators, Interleukin-6 receptor antagonists in critically Ill patients with Covid-19. *N. Engl. J. Med.* **384**, 1491–1502 (2021).
32. M. Martin-Fernandez, L. M. Vaquero-Roncero, R. Almansa, E. Gómez-Sánchez, S. Martín, E. Tamayo, M. C. Esteban-Velasco, P. Ruiz-Granado, M. Aragón, D. Calvo, J. Rico-Feijoo, A. Ortega, E. Gómez-Pesquera, M. Lorenzo-López, J. López, C. Doncel, C. González-Sanchez, D. Álvarez, E. Zarca, A. Ríos-Llorente, A. Diaz-Alvarez, E. Sanchez-Barrado, D. Andaluz-Ojeda, J. M. Calvo-Vecino, L. Muñoz-Bellvís, J. I. Gomez-Herreras, C. Abad-Molina, J. F. Bermejo-Martin, C. Aldecoa, M. Heredia-Rodríguez, Endothelial dysfunction is an early indicator of sepsis and neutrophil degranulation of septic shock in surgical patients. *BJS Open* **4**, 524–534 (2020).
33. J. J. Presneill, P. M. Waring, J. E. Layton, D. W. Maher, J. Cebon, N. S. Harley, J. W. Wilson, J. F. Cade, Plasma granulocyte colony-stimulating factor and granulocyte-macrophage colony-stimulating factor levels in critical illness including sepsis and septic shock: Relation to disease severity, multiple organ dysfunction, and mortality. *Crit. Care Med.* **28**, 2344–2354 (2000).
34. A. Fuchs, D. A. Monlish, S. Ghosh, S. W. Chang, G. V. Bochicchio, L. G. Schuettpelz, I. R. Turnbull, Trauma induces emergency hematopoiesis through IL-1/MyD88-dependent production of G-CSF. *J. Immunol.* **202**, 3020–3032 (2019).
35. F. Veglia, E. Sanseviero, D. I. Gabrilovich, Myeloid-derived suppressor cells in the era of increasing myeloid cell diversity. *Nat. Rev. Immunol.* **21**, 485–498 (2021).
36. I. T. Schrijver, C. Théroude, T. Roger, Myeloid-derived suppressor cells in sepsis. *Front. Immunol.* **10**, 327 (2019).
37. M. A. O'Connor, J. L. Rastad, W. R. Green, The role of myeloid-derived suppressor cells in viral infection. *Viral Immunol.* **30**, 82–97 (2017).
38. R. S. Tacke, H.-C. Lee, C. Goh, J. Courtney, S. J. Polyak, H. R. Rosen, Y. S. Hahn, Myeloid suppressor cells induced by hepatitis C virus suppress T-cell responses through the production of reactive oxygen species. *Hepatology* **55**, 343–353 (2012).
39. A. Sacchi, G. Grassi, V. Bordoni, P. Lorenzini, E. Cimini, R. Casetti, E. Tartaglia, L. Marchioni, N. Petrosillo, F. Palmieri, G. D'Offizi, S. Notari, M. Tempestilli, M. R. Capobianchi, E. Nicastri, M. Maeurer, A. Zumla, F. Locatelli, A. Antinori, G. Ippolito, C. Agrati, Early expansion of myeloid-derived suppressor cells inhibits SARS-CoV-2 specific T-cell response and may predict fatal COVID-19 outcome. *Cell Death Dis.* **11**, 921 (2020).
40. S. Falck-Jones, S. Vangeti, M. Yu, R. Falck-Jones, A. Cagigi, I. Badolati, B. Österberg, M. J. Lautenbach, E. Åhlberg, A. Lin, R. Lepzien, I. Szurgot, K. Lenart, F. Hellgren, H. Maecker, J. Sälde, J. Albert, N. Johansson, M. Bell, K. Loré, A. Färnert, A. Smed-Sörensen, Functional monocytic myeloid-derived suppressor cells increase in blood but not airways and predict COVID-19 severity. *J. Clin. Invest.* **131**, e144734 (2021).
41. Y. V. Perfilyeva, Y. O. Ostapchuk, R. Tleulieva, A. Kali, N. Abdolla, V. K. Krasnoshtanov, A. V. Perfilyeva, N. N. Belyaev, Myeloid-derived suppressor cells in COVID-19: A review. *Clin. Immunol.* **238**, 109024 (2022).
42. L. E. Cabrera, P. T. Pekkarinen, M. Alander, K. H. A. Nowlan, N. A. Nguyen, S. Jokiranta, S. Kuivanen, A. Patjas, S. Mero, S. H. Pakkanen, S. Heinonen, A. Kantele, O. Vapalahti, E. Kekäläinen, T. Strandin, Characterization of low-density granulocytes in COVID-19. *PLOS Pathog.* **17**, e1009721 (2021).
43. S. M. Morrissey, A. E. Geller, X. Hu, D. Tieri, C. Ding, C. K. Klaes, E. A. Cooke, M. R. Woeste, Z. C. Martin, O. Chen, S. E. Bush, H.-G. Zhang, R. Cavallazzi, S. P. Clifford, J. Chen, S. Ghare, S. S. Barve, L. Cai, M. Kong, E. C. Rouchka, K. R. McLeish, S. M. Uriarte, C. T. Watson, J. Huang, J. Yan, A specific low-density neutrophil population correlates with hypercoagulation and disease severity in hospitalized COVID-19 patients. *JCI Insight* **6**, e148435 (2021).
44. S. Sinha, N. L. Rosin, R. Arora, E. Labit, A. Jaffer, L. Cao, R. Farias, A. P. Nguyen, L. G. N. de Almeida, A. Dufour, A. Bromley, B. McDonald, M. R. Gillrie, M. J. Fritzler, B. G. Yipp, J. Biernaskie, Dexamethasone modulates immature neutrophils and interferon programming in severe COVID-19. *Nat. Med.* **28**, 201–211 (2022).
45. M. Merad, J. C. Martin, Pathological inflammation in patients with COVID-19: A key role for monocytes and macrophages. *Nat. Rev. Immunol.* **20**, 355–362 (2020).
46. P. A. Szabo, P. Dogra, J. I. Gray, S. B. Wells, T. J. Connors, S. P. Weisberg, I. Krupska, R. Matsumoto, M. M. L. Poon, E. Idzikowski, S. E. Morris, C. Pasin, A. J. Yates, A. Ku, M. Chait, J. Davis-Porada, X. V. Guo, J. Zhou, M. Steinle, S. Mackay, A. Saqi, M. R. Baldwin, P. A. Sims, D. L. Farber, Longitudinal profiling of respiratory and systemic immune responses reveals myeloid cell-driven lung inflammation in severe COVID-19. *Immunity* **54**, 797–814.e6 (2021).
47. L. B. Boyette, C. Macedo, K. Hadi, B. D. Elinoff, J. T. Walters, B. Ramaswami, G. Chalasani, J. M. Taboas, F. G. Lakkis, D. M. Metes, Phenotype, function, and differentiation potential of human monocyte subsets. *PLOS ONE* **12**, e0176460 (2017).
48. L. Vanderbeke, P. van Mol, Y. van Herck, F. de Smet, S. Humblet-Baron, K. Martinod, A. Antoranz, I. Arijs, B. Boeckx, F. M. Bosisio, M. Casaer, D. Dauwe, W. de Wever, C. Dooms, E. Dreesen, A. Emmaneel, J. Filtjens, M. Gouwy, J. Gunst, G. Hermans, S. Jansen, K. Lagrou, A. Liston, N. Lorent, P. Meersseman, T. Mercier, J. Neyts, J. Odent, D. Panovska, P. A. Penttila, E. Pollet, P. Proost, J. Qian, K. Quintelier, J. Raes, S. Rex, Y. Saeys, J. Sprooten, S. Tejpar, D. Testelmans, K. Thevissen, T. van Buyten, J. Vandenhaute, S. van Gassen, L. C. Velásquez Pereira, R. Vos, B. Weynand, A. Wilmer, J. Yserbyt, A. D. Garg, P. Matthys, C. Wouters, D. Lambrechts, E. Wauters, J. Wauters, Monocyte-driven atypical cytokine storm and aberrant neutrophil activation as key mediators of COVID-19 disease severity. *Nat. Commun.* **12**, 4117 (2021).
49. I. Sánchez-Cerrillo, P. Landete, B. Aldave, S. Sánchez-Alonso, A. Sánchez-Azofra, A. Marcos-Jiménez, E. Ávalos, A. Alcaraz-Serna, I. de Los Santos, T. Mateu-Albero, L. Esparcia, C. López-Sanz, P. Martínez-Fleta, L. Gabrie, L. D. C. Guerola, H. de la Fuente, M. J. Calzada, I. González-Álvaro, A. Alfranca, F. Sánchez-Madrid, C. Muñoz-Calleja, J. B. Soriano, J. Ancochea, E. Martín-Gayo; REINMUN-COVID and EDEPIMIC groups, COVID-19 severity associates with pulmonary redistribution of CD1c+ DCs and inflammatory transitional and nonclassical monocytes. *J. Clin. Invest.* **130**, 6290–6300 (2020).
50. F. Venet, J. Demaret, M. Gossez, G. Monneret, Myeloid cells in sepsis-acquired immunodeficiency. *Ann. N. Y. Acad. Sci.* **1499**, 3–17 (2021).
51. D. P. Zhang, F. L. Yan, H. Q. Xu, Y. X. Zhu, Y. Yin, H. Q. Lu, A decrease of human leucocyte antigen-DR expression on monocytes in peripheral blood predicts stroke-associated infection in critically-ill patients with acute stroke. *Eur. J. Neurol.* **16**, 498–505 (2009).
52. H. Diao, G. Cui, Y. Wei, J. Chen, J. Zuo, H. Cao, Y. Chen, H. Yao, Z. Tian, L. Li, Severe H7N9 infection is associated with decreased antigen-presenting capacity of $CD14^+$ cells. *PLOS ONE* **9**, e92823 (2014).
53. M. Wieczorek, E. T. Abualrous, J. Sticht, M. Álvaro-Benito, S. Stolzenberg, F. Noé, C. Freund, Major histocompatibility complex (MHC) class I and MHC class II proteins: Conformational plasticity in antigen presentation. *Front. Immunol.* **8**, 292 (2017).
54. G. Xue, M. Jiang, R. Zhao, A. Le, J. Li, Elevated frequencies of $CD14^+HLA\text{-}DR^{lo/neg}$ MDSCs in COVID-19 patients. *Aging (Albany NY)* **13**, 6236–6246 (2021).
55. M. Reyes, M. R. Filbin, R. P. Bhattacharyya, A. Sonny, A. Mehta, K. Billman, K. R. Kays, M. Pinilla-Vera, M. E. Benson, L. A. Cosimi, D. T. Hung, B. D. Levy, A. C. Villani, M. Sade-Feldman, R. M. Baron, M. B. Goldberg, P. C. Blainey, N. Hacohen, Plasma from patients with bacterial sepsis or severe COVID-19 induces suppressive myeloid cell production from hematopoietic progenitors in vitro. *Sci. Transl. Med.* **13**, abe9599 (2021).

**Acknowledgments:** We would like to acknowledge the NIH Clinical Center Department of Laboratory Medicine for the processing of laboratories associated with the treatment of patients in this trial. We would also like to acknowledge A. Saxena and P. J. McCoy from the National Heart, Lung, and Blood Institute (NHLBI) Flow Cytometry Core for their work relating to cytokine analysis in this study. **Funding:** This work has been funded in part by the Intramural Research Program of the NIH Clinical Center (NIHCC) including a Research Award for Staff Clinicians (FY2020/FY2021), NHLBI, National Institute of Allergy and Infectious Diseases (NIAID), and National Institute of Arthritis and Musculoskeletal and Skin Diseases (NIAIMS). Support for clinical fostamatinib phase 2 clinical trial was provided though a Cooperative Research and Development Agreement (CRADA) between the NHLBI and Rigel Pharmaceuticals. The opinions expressed in this article are those of the authors and do not represent any position or policy of the NIH, the U.S. Department of Health and Human Services, or the U.S. government. **Author contributions:** Conceptualization: G.W., L.K., S.M., R.W.C., M.J.K., D.S.C., and J.R.S. Methodology: G.W., S.A.W., M.J.R.-B., L.K., X.T., Y.K., S.M., R.W.C., M.J.K., D.S.C., and J.R.S. Investigation: G.W., SA.W., M.J.R.-B., L.K., X.T., R.R., M.C., S.W., Y.K., A.F.S., S.D., S.B., C.K., O.S., S.D.N., J.C., S.M., R.W.C., M.J.K., D.S.C., and J.R.S. Visualization: G.W., M.J.R.-B., L.K., and J.R.S. Funding acquisition: S.M., R.W.C., M.J.K., D.S.C., and J.R.S. Supervision: S.M., M.J.K., D.S.C., and J.R.S. Writing—original draft: G.W. and J.R.S. Writing—review and editing: All authors. **Competing interests:** The authors declare that they have no competing interests. **Data and materials availability:** All data needed to evaluate the conclusions in the paper are present in the paper and/or the Supplementary Materials.

Submitted 10 September 2022
Accepted 23 November 2022
Published 4 January 2023
10.1126/sciadv.ade8272